ACS Chemical Neuroscience

Article

Dopamine D3/D2 Receptor Antagonist PF-4363467 Attenuates Opioid Drug-Seeking Behavior without Concomitant D2 Side Effects

Travis T Wager, Thomas A. Chappie, David Horton, Ramalakshmi Y. Chandrasekaran, Brian M. Samas, Elizabeth Dunn-Sims, Cathleen Hsu, Nawshaba Nawreen, Michelle A Vanase-Frawley, Rebecca E O'Connor, Christopher Schmidt, Keith Dlugolenski, Nancy C. Stratman, Mark J. Majchrzak, Bethany L. Kormos, David Nguyen, Aarti Sawant-Basak, and Andy N. Mead

ACS Chem. Neurosci., **Just Accepted Manuscript** • DOI: 10.1021/acschemneuro.6b00297 • Publication Date (Web): 07 Oct 2016

Just Accepted

ACS Publications

ACS Chemical Neuroscience is published by the American Chemical Society. 1155 Sixteenth Street N.W., Washington, DC 20036

Dopamine D3/D2 Receptor Antagonist PF-4363467 Attenuates Opioid Drug-Seeking Behavior without Concomitant D2 Side Effects

Travis T. Wager, Thomas Chappie, David Horton, Ramalakshmi Y. Chandrasekaran, Brian Samas, Elizabeth R. Dunn-Sims, Cathleen Hsu, Nawshaba Nawreen, Michelle A. Vanase-Frawley, Rebecca E. O'Connor, Christopher J. Schmidt, Keith Dlugolenski, Nancy C. Stratman, Mark J. Majchrzak, Bethany L. Kormos, David Nguyen, Aarti Sawant-Basak, Andy N. Mead

Pfizer Worldwide Research and Development; Neuroscience Medicinal Chemistry and Neuroscience Research Unit, 610 Main Street, Cambridge, MA 02139 (TTW, TC, CJS, KD, NCS, BLK); Pharmacokinetics, Dynamics, and Metabolism, 610 Main Street, Cambridge, MA 02139 (DN, AS-B); Chemistry and Biology, Eastern Point Road, Groton, CT 06340 (RYC, BS DH, ERD-S, CH, NN, MJM ANM, MAV-F, REO).

ABSTRACT: Dopamine receptor antagonism is a compelling molecular target for the treatment of a range of psychiatric disorders, including substance use disorders. From our corporate compound file we identified a structurally unique D3 receptor (D3R) antagonist scaffold, **1**. Through a hybrid approach, we merged key pharmacophore elements from **1** and D3 agonist **2** to yield the novel D3R/D2R antagonist PF-4363467 (**3**). Compound **3** was designed to possess CNS drug-like properties as defined by its CNS MPO desirability score (≥4/6). In addition to good physicochemical properties, **3** exhibited low nanomolar affinity for the D3R (D3 K_i = 3.1 nM), good subtype selectivity over D2R (D2 K_i = 692 nM), and high selectivity for D3R versus other biogenic amine receptors. In vivo, **3** dose-dependently attenuated opioid self-

administration and opioid drug-seeking behavior in a rat operant reinstatement model using animals trained to self-administer fentanyl. Further, traditional extrapyramidal symptoms (EPS), adverse side effects arising from D2R antagonism, were not observed despite high D2 receptor occupancy (RO) in rodents, suggesting that compound **3** has a unique in vivo profile. Collectively, our data support further investigation of dual D3R and D2R antagonists for the treatment of drug addiction.

KEYWORDS: Substance use dependence, drug addiction, CNS MPO, dopamine D3 antagonist, dopamine D2 antagonist, opioid, cessation, drug-seeking behavior, reinstatement, extrapyramidal symptoms, locomotor.

[a]Abbreviations: ADME, absorption, distribution, metabolism and excretion; CK1, casein kinase 1; AUC, area under the curve; C_{ave}, average concentration; C_{eff}, efficacious concentration; C_{max}, maximum concentration; CNS, central nervous system; CPP, conditioned place preference; DA, dopamine; D2R, dopamine 2 receptor; D3R, dopamine 3 receptor; EPS, extrapyramidal symptoms; HBD, hydrogen bond donor; HLM, human liver microsomes; ICSS, intracranial self-stimulation; MDR, multi-drug resistance; MPO, multi-parameter optimization; P-gp, P-glycoprotein; SAR, structure-activity relationship; SBDD, structure-based drug design.

Introduction

Drug addiction is characterized as compulsive, out-of-control drug use despite negative consequences including significant morbidity and mortality. Substance abuse is a global health concern with major socio-economic ramifications, which has reached epidemic proportions. For example, opioid dependency increased 74% from 1990 through 2010 and the economic cost

attributable to illicit drug use in the United States alone is estimated to be over $500 billion annually.[1, 2] Opioid dependency is particularly troubling in that it accounted for nearly half the estimated 20 million disability-adjusted life years worldwide for illicit drug use in 2010 and more than half of the 78,000 deaths in 2010 due to illicit drug use.[2] Furthermore, recent trends suggest that opioid addiction afflicts young people (ages 15–29), a population that will likely carry this burden of drug dependency throughout life. Given the continued rise in opioid dependency, there is an urgent need to develop new medicines that can be used both to treat addiction and to prevent relapse.

We recently disclosed that casein kinase 1 inhibitors (CK1i) attenuate opioid-seeking behavior in a rodent reinstatement model of fentanyl self-administration.[3] While CK1 inhibition is an attractive target for the treatment of drug addiction, dopamine (DA) receptor antagonism is also a compelling molecular target, given the rich preclinical and clinical literature data on this approach. In particular, the dopamine D3 receptor (D3R) has been pursued for more than a decade as a potential target for the treatment of substance use disorders,[4, 5] with numerous groups developing selective ligands targeting D3R.[6-8] Several lines of evidence provide a rationale to target D3R and D2 receptors (D2R) for the treatment of substance abuse disorders. D3R and D2R are distributed in key brain regions that regulate the rewarding, motoric, cognitive, and emotional effects of opioids. D2R expression is widespread in the brain, with the highest concentration found in the striatum, followed by the nucleus accumbens, globus pallidus, subtantia nigra and ventral tegmental area.[9] Conversely, D3R is most abundant in the globus pallidus, ventral pallidum/substantia innominata, and substantia nigra, which have all been associated with motivational processing and are likely part of the neurocircuitry of addiction and relapse.[9-11] In contrast to D2R, D3R is virtually absent in the ventral tegmental area, which is

associated with a rewarding response to low-dose opioid injections.[12] Blockade of D2R in the ventral tegmental area may help reduce opioid use. Further, there is evidence that abnormal D2R expression and function can provide a pre-existing vulnerability, in addition to arising as a consequence of substance abuse disorder.[13] Co-expression of D2R and D3R in many brain regions suggests a functional convergence of the signals mediated by these receptors.[9] The brain regions that express D2R and D3R have been shown to be important for motivation and reward, as well as drug-mediated and cue-induced relapse. Thus, the localization of these receptors in these brain regions suggests a potential role for modulating addictive behaviors.

Repeated exposure to illicit drugs produces long-term molecular and neurochemical changes in the brain in both humans and animals.[14] Postmortem evaluation of the expression of D3R in the brains of chronic cocaine users revealed an increased receptor density when compared with age-matched and drug-free control subjects.[15-17] This observation of increased receptor density has been extended to other drugs of abuse, including methamphetamine and alcohol.[18, 19] The up-regulation of D3R in the addicted state suggests a role for D3R in the neuroadaptive responses to addictive drugs, and implies that blocking D3R may reduce craving and relapse rates.

Recent literature suggests that D3R/D2R ligands have potential efficacy in blocking drug-seeking behavior in both preclinical and clinical models of addiction.[6, 20-22] Early work examining the effect of D3R preferential agonists on cocaine self-administration in rats revealed the importance of D3Rs in the reinforcing effects of cocaine.[23] Further research has shown that BP 897, a D3R partial agonist, dose-dependently reduced cocaine seeking;[20] additional studies, however, have shown that this compound exhibits antagonism at D3R.[24] More recently, Román et al. reported that cariprazine, a 10-fold selective D3R/D2R partial agonist, was able to reduce

the rewarding effect of cocaine and to attenuate relapse to cocaine-seeking in rats.[21] Further work with antagonists has shown that SB-277011-A, a D3R/D2R antagonist, inhibits both cocaine-conditioned place preference (CPP) and reinstatement of cocaine-seeking behavior, as well as cocaine-induced increases in brain stimulation reward.[25] NGB 2904, a selective D3R antagonist, was reported to inhibit cocaine self-administration under a progressive ratio schedule, reinstatement of cocaine-seeking behavior, and enhancement of brain stimulation reward induced by cocaine, methamphetamine, heroin, and nicotine.[26] Others have disclosed the discovery of novel selective D3R antagonists and reported the potential utility of D3R antagonist in treating opioid addiction.[27-30] Finally, the selective D3R antagonist GSK598809 dose-dependently attenuated nicotine-induced CPP in rats; this effect translated into the clinic, where GSK598809 transiently alleviated craving in smokers at sub-maximal receptor occupancy (72–89%).[31] This investigation provided the first clinical evidence supporting the hypothesis that D3R antagonism would be effective in treating substance use disorders.

Given the growing preclinical and clinical data arising from subtype-preferring D3R/D2R antagonists and selective D3R antagonists, antagonism of these receptors might be a promising approach to treat substance abuse disorders and addiction. High DA receptor subtype selective D3R antagonists are ideal for preclinical study of the specific role of D3R in addiction; however, they may fall short of desired outcomes in the clinic due to the complex nature of addiction and dopamine signaling. For this reason we pursued compounds that had the potential to engage D3R at high occupancy levels, while simultaneously interacting with D2R at a wide range of occupancies, given the potentially significant roles that both D3R and D2R play in addiction. Based on the receptor occupancy achieved in the GSK598809 clinical study, and our knowledge of D2R-related EPS effects, our initial target was a compound that could achieve high D3

receptor occupancy (>90%) with low D2 receptor occupancy (<10%). A second objective was to establish whether it was possible to titrate in higher D2R occupancy and thereby achieve improved efficacy in rodent models of substance use and relapse disorders. We hypothesized that this dual-pharmacology strategy would improve efficacy by broadening the modulatory influence over cue-reward processing pathways.

Results and Discussion

Our re-entry into identifying subtype-selective D3R antagonists began with a review of our corporate file, which at the time included compounds from legacy Pfizer and Pharmacia & Upjohn D3R and D2R antagonist and agonist programs; these analogues had been assayed for binding and functional activity. Of the compounds that were in the file, PNU-177864 (**1**) represented a structurally unique D3R antagonist scaffold (Table 1).[32] Structurally, **1** had an aryl sulphonamide, distinguishing it from many of the published selective D3R antagonists, which often contained an aryl-piperidine moiety.[33] Compound **1** exhibited moderate affinity for D3R and good selectivity over D2R (Table 1) and was shown to be a functional antagonist, as measured by a human D3 SH-SY5Y GTP-γ-S functional assay. The known in vivo phospholipidosis safety liability of **1** prompted us to identify an amine replacement.[32] Specifically, we wanted to reduce the pK_a of the basic amine and lower the lipophilicity of the compound. This approach has been successfully applied in a histamine H3 receptor program to reduce phospholipidosis liability, and resulted in the identification of two clinical candidates.[34] At this point we revisited our corporate file, seeking other D3R ligands with predicted pK_a < 9 for the most basic center. PF-592379 (**2**) was identified as a potential lead that retained affinity and selectivity for D3R over D2R, although functionally it was a full agonist (Table 1).[35] The physicochemical properties of **2** were significantly better than those of **1** (Table 2), thus allowing

for considerable structural modification opportunities with which to switch the in vitro functional activity from agonist to antagonist.

Hybridization of **1** and **2**, along with application of traditional structure activity relationships (SAR), led to the identification of PF-4363467 (**3**) and its enantiomer PF-4363476 (not shown) (Table 1). Compound **3** exhibited single digit nM affinity for D3R (K_i = 3.1 nM) and greater than 100-fold selectivity over D2R (K_i = 692 nM; Table 1). Further, **3** was an antagonist in the human D3 SH-SY5Y GTP-γ-S functional assay and in the human D2 SH-SY5Y cAMP stimulation assay (Table 1). Functional D2/D3 selectivity was in line with binding selectivity, thus achieving our initial goal of a novel D3-selective antagonist.

Table 1. Corporate file mining leads and hybrid compound **3**.

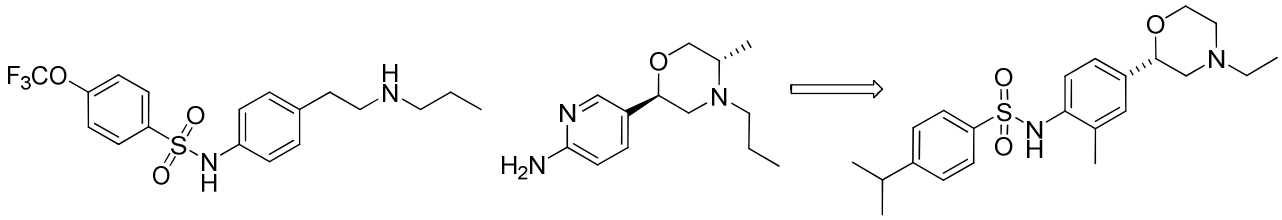

1 (PNU-177864) **2** (PF-592379) **3** (PF-4363467)

ID	D3 K_i (nM)[a]	D2 K_i (nM)[a]	D2/ D3	D3 Functional (nM)[b]	D2 Functional (nM)[b]	Functional Activity
1	38.2 (23.6 – 61.9)	4480 (3290 – 6090)	117	K_i = 22 (10.1 - 48.9)[c]	K_i > 33[c]	Antagonist
2	322 (57.9 – 1790)	>4160	>12	EC_{50} = 21[d]	EC_{50} > 9,000[d]	Agonist
3	3.1 (2.47 – 3.99)	692 (539 – 890)	223	K_i = 1.1 (0.61 - 2.1)[c]	K_i = 464 (188 – 1147)[c]	Antagonist

[a]Human dopamine D3 and D2 binding data reported as the geometric mean of at least 3 determinations. [b]Human dopamine D3 and D2 functional data reported as the geometric mean of at least 3 determinations. [c]Data reported as mean antagonist activity with (95% CI). [d]Data reported by Attkins et al.[35] as agonist activity.

The overall physicochemical properties of **3** are in line with marketed CNS drugs, with a CNS multi-parameter optimization (CNS MPO) desirability score of 4.0/6.0 (Table 2).[36-38] Improvements in ClogP, HBD, and pK_a were achieved relative to compound **1**; most notable is the change in pK_a, which was lowered from 10.6 to 7.5. ClogD7.4 is still relatively high for **3** (ClogD7.4 = 3.96, which may be a contributing factor in its high human liver microsome (HLM) clearance (Table 3). Future work around this chemotype should focus on further lowering ClogP and ClogD7.4, with a goal of improving CNS MPO desirability and aligning all ADME attributes to desirable values.

Table 2. Summary of physicochemical properties and CNS MPO desirability

	Compound **1**		Compound **2**		Compound **3**	
Physicochemical Property	Value	Component Score	Value	Component Score	Value	Component Score
MW	402	0.70	235	1.00	403	0.70
ClogP	4.46	0.27	1.48	1.00	4.06	0.47
TPSA	67.4	1.00	51.4	1.00	58.6	1.00
ClogD7.4	1.06	1.00	0.76	1.00	3.96	0.02
HBD	2	0.50	2	0.50	1	0.83
pK_a	10.6	0.00	7.5	1.00	7.5	1.00
CNS MPO		3.5/ 6.0		5.5/ 6.0		4.0/ 6.0

[a]Calculated CNS MPO desirability scores were obtained using the published algorithm.[37] Color code for component score (x): red, $x \leq 0.33$; yellow, $0.33 < x \leq 0.66$; green, $x > 0.66$.

In addition to good physicochemical properties and potency, compound **3** exhibited good passive permeability, with a P_{app} value of 8.4×10^{-6} cm/sec and predicted low-to-moderate P-gp liability (Table 3). Brain availability ($C_{b,u}/C_{p,u}$) in rats was 1.0 and free brain exposure of **3** ($C_{max,b,u}$) at a 10 mg/kg s.c. dose was determined to be 23.7 nM. At a 10 mg/kg s.c. dose, **3** had sufficient free drug exposure to cover the D3R K_i (~7 fold). $C_{max,b,u}$ was further used to estimate target occupancy (%) as:

$$Target\ Occupancy = \frac{C_{max,b,u}}{C_{max,b,u} + K_d} \bullet 100 \quad (1)$$

where the dissociation constant K_d represents in vitro target binding potency. Using the binding K_i as a surrogate for K_d, compound **3** was initially estimated to have maximum CNS target occupancy of 88% for D3R and 5% for D2, after a 10 mg/kg s.c. dose.

Table 3. Summary of ADME properties for **3**.

Compound	HLM[a]	P_{app}[b]	P-gp[c]	Rat $C_{max,b,u}$ [nM][d]	Rat $AUC_{0-\infty}$ C_b/C_p	Rat $AUC_{0-\infty}$ $C_{b,u}/C_{p,u}$
3	126	8.4	2.3	23.7	2.4	1.01

[a]Human liver microsomal clearance (μL/min/mg). [b]Passive permeability (P_{app} AB x 10^{-6} cm/sec). [c]MDR1 Efflux Ratio (BA/AB). [d]Rat $C_{max,b,u}$ values are reported as maximum free drug concentration in brain at a 10 mg/kg dose, s.c.

Compound **3** was further evaluated in a broad selectivity panel, where it demonstrated high selectivity for D3R over receptors for other biogenic amines, ion channels, and enzymes (Figure 1, see supplementary material, Table 1s for details). In this 129-target selectivity panel, **3** inhibited 22 targets at >50% inhibition at 10 μM drug concentration. Of the off-target activities tested in IC_{50} format, **3** had the highest affinity for CYP2C19 (110 nM, 34-fold higher than the D3R binding IC_{50}), followed by 5HT6 (990 nM, 309-fold higher than the D3R IC_{50}) and 5HT2A (1.4 μM, 437-fold higher than the D3R IC_{50}). Overall, compound **3** possessed an excellent selectivity profile and was therefore progressed into ex vivo brain target occupancy studies.

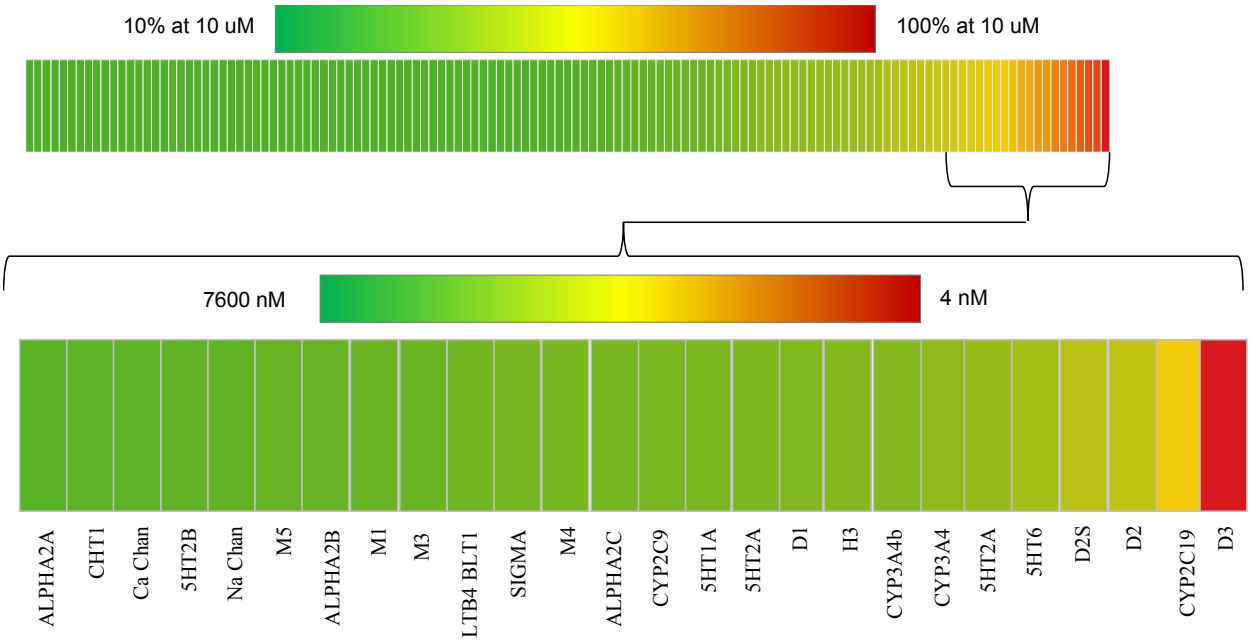

Figure 1. A) Percent inhibition of a 129-target promiscuity panel at 10 μM of compound **3**. Heat map colors for this continuum: green, 0% inhibition; yellow, 50% inhibition; red, 100% inhibition. B) IC_{50} determination for 26 targets hitting in the promiscuity panel with inhibition >50% for compound **3**. Heat map colors continuum: green, 7,600 nM; yellow, 100 nM and red, 4 nM. IC_{50} determinations for the 10 highest affinity targets for compound **3** were: D3R, 4 nM; CYP2C19, 110 nM; D2R, 420 nM; D2S, 540 nM; 5HT6, 990 nM; 5HT2A, 1400 nM; CYP3A4b, 2300 nM; H3, 2400 nM; D1R, 2500 nM.

Using an ex vivo autoradiography technique with rat brain slices, compound **3** was evaluated for both D3R and D2R occupancy (Table 4, Figure 2A, 2B). The 0.1 mg/kg dose resulted in moderate D3R occupancy (33.6%) and low D2R occupancy (10.8%). High D3R occupancy was achieved at the 3.2 mg/kg dose with near maximal occupancy (>95%) and moderate D2R occupancy (34.7%). It was not until 32 mg/kg that D2R occupancy was over 75%. The ex vivo receptor occupancy EC_{50} was determined to be 1.5 nM for D3R and 46.6 nM for D2R. The D3R occupancy EC_{50} is within 3-fold of the binding K_i; however, the D2R

occupancy EC_{50} is 10-fold left-shifted when compared to the in vitro binding K_i. This was the first piece of data that suggested this compound does not behave like a traditional D3/D2 antagonist (i.e. eticlopride and sulpiride). The ex vivo D3R and D2R occupancy characteristics of **3** represented a reasonable profile to test two hypotheses with one molecule, simply by varying the dose. First, can a selective D3R antagonist (low dose) attenuate opioid drug-seeking behavior or, second, is dual pharmacology required (high dose) to yield a robust in vivo biological response?

Table 4. D3R and D2R brain receptor occupancy from autoradiography techniques in rats

Compound	Treatment (mg/kg)	$C_{max,b,u}$ (nM)	D3 EVRO % RO Observed[a]	D2 EVRO % RO Observed[b]
3	32	207.1	---	85.9 ± 1.7
	10	43.9	98.8 ± 2.4	50.6 ± 3.5
	3.2	13.6	99.9 ± 0.5	34.7 ± 1.5
	0.1	0.7	33.6 ± 4.5	10.8 ± 4.1
	0.032	0.2	6.3 ± 10.1	---
		EC_{50}	1.5 ± 0.4 nM	46.6 ± 9.1 nM

[a]Brain region evaluated: rat cerebellum (mean ± SEM, n = 3–4). [b]Brain region evaluated: rat striatum (mean ± SEM, n = 4). Ex vivo Receptor Occupancy (EVRO).

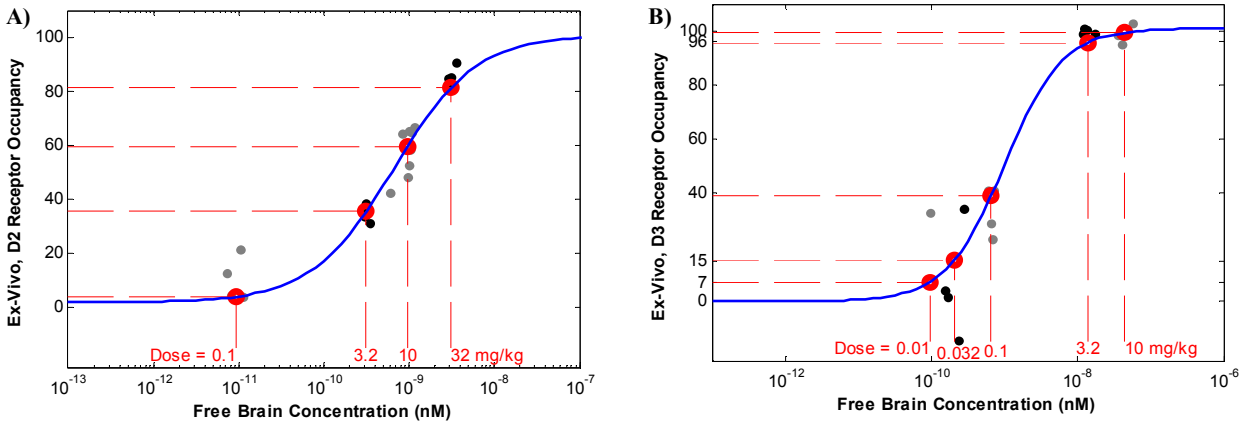

Figure 2. A) D2 (striatum) and B) D3 (cerebellum) brain receptor occupancy curves from the ex vivo autoradiography protocol in rat. The gray and black data points represent actual measured

RO and brain PK from individual animals. The solid line is the data-fitted RO model. The D3R binding was measured in cerebellum, while the D2R binding was measured in striatum.

Given the higher-than-expected D2R occupancy in the ex vivo receptor occupancy assay, we were concerned that significant D2R side effects would be observed at low doses (≤10 mg/kg). Haloperidol and other D2R antagonists provoke prolactin secretion and elicit catalepsy in preclinical and clinical studies.[39-42] The induction of catalepsy in rat preclinical studies is believed to be a predictor of extrapyramidal syndrome (EPS) in man. Further, it has been suggested that D2R antagonism may decrease locomotor activity.[43] Prolactin serves as a marker for D2R antagonism and the magnitude of response is roughly correlated with the occupancy of D2 receptors in the pituitary.[44, 45] As expected, **3** (0.1–10 mg/kg) dose-dependently increases prolactin release in rats (Figure 3A). At the highest dose tested in rats (10 mg/kg), **3** increases plasma prolactin 9.3-fold ($p < 0.05$). Unexpectedly, compound **3** had no significant effects on spontaneous locomotor activity (Figure 3B) at the highest dose tested (32 mg/kg), where D2R occupancy is 85.9%. Further, **3** did not produce a statistically significant cataleptic effect in rats at any dose tested up to a dose of 32 mg/kg (Figure 3C). While this was surprising, there have been reports of selective D3R antagonists attenuating catalepsy induced by haloperidol.[46] The lack of significant locomotor and catalepsy side effects after administration of **3** make this a unique compound, and we undertook further evaluations to determine whether there are advantages of dosing **3** to both high D3R and D2R occupancy in models of addiction.

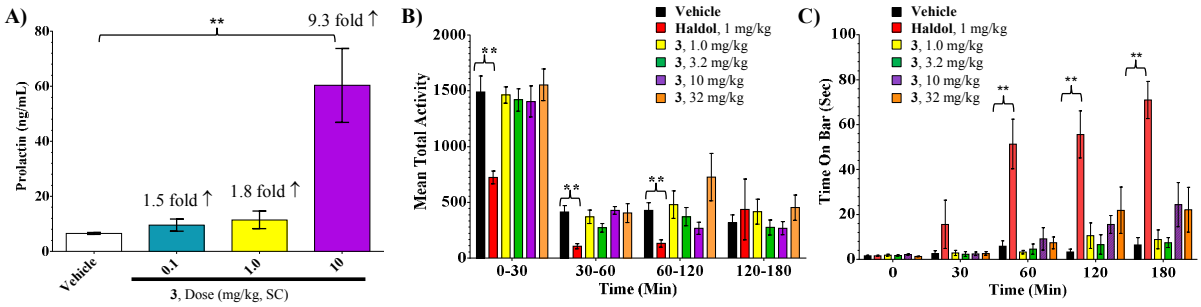

Figure 3. A) Effect of **3** on prolactin. Data represent mean ± SEM, *n* = 5/group. B) Effects of **3** on total activity in a rat model of locomotor activity. Data represent mean ± SEM locomotor activity over 30 minute time bins, *n* = 8/group. C) Effects of **3** in a rat model of catalepsy. Data represents mean ± SEM seconds on bar demonstrating the effect of **3** (1.0–32.0 mg/kg, s.c.), *n* = 8/group. ** indicates $p < 0.01$ compared to vehicle group.

To evaluate the utility of D3R/D2R antagonism in substance use disorder treatment, the effect of **3** was assessed in both a cessation model of drug-taking (Figure 4A) and a relapse model of drug-seeking behavior (Figure 4B). With respect to cessation, administration of **3** reduced self-administration of fentanyl (Figure 4A), as indicated by a significant main effect of dose ($F_{(4, 312)} = 23.93$, $p < 0.0001$), a significant main effect of session ($F_{(6,312)} = 8.14$, $p < 0.0001$) and a significant dose by session interaction ($F_{(24,312)} = 2.64$, $p < 0.0001$). Follow-up analysis of infusions for each test session by one-way ANOVA revealed a significant main effect of dose across sessions 1, 2, and 3 ($F_{(4,37)} = 7.47$, $p<0.001$; $F_{(4,37)} = 6.89$, $p < 0.001$; $F_{(4,37)} = 11.2$, $p < 0.0001$, respectively). Post hoc comparisons at each test session revealed a significant decrease in infusions following pretreatment with 32 mg/kg of **3** for all three sessions ($p < 0.001$) and when fentanyl was replaced with saline under the saline extinction condition for sessions 1 and 3 ($p < 0.05$ and $p < 0.01$, respectively). Analysis of the average infusions obtained over three consecutive test days in the fentanyl cessation model following treatment with **3** revealed a

significant main effect of dose ($F_{4,37}$ = 10.8, p < 0.0001) and post hoc comparisons indicated a significant decrease in average infusions following pretreatment of 32 mg/kg and when fentanyl was replaced with saline (saline extinction) compared to when fentanyl was available for self-administration (vehicle; Figure 1s, supporting information). A trend for a reduction in fentanyl self-administration was observed following 10 mg/kg of **3**, but the effect did not reach statistical significance (p = 0.08).

To further determine the effect of **3** on fentanyl-seeking behavior, the ability of **3** to attenuate reinstatement of fentanyl seeking was assessed, following exposure to both a fentanyl drug prime and fentanyl-associated cues. Analysis of results revealed a main effect of dose ($F_{(3,21)}$ = 3.28; $p < 0.05$), a main effect of test ($F_{(1,7)}$ = 7.66; $p < 0.05$) and a significant dose by test interaction ($F_{(3,21)}$ = 3.32; $p < 0.05$; Figure 4B). Post hoc comparisons revealed a significant reinstatement effect following administration of 3.2 ($t_{(7)}$ = −2.52; p < 0.05) and 10 mg/kg ($t_{(7)}$ = −2.94; p < 0.05) of **3** compared to baseline, with a strong trend for an increase following vehicle pretreatment (p = 0.058). While the effect of vehicle on reinstatement was just outside significance, normalization of the active lever responses to fentanyl intake obtained during the last two sessions of fentanyl self-administration training (Figure 2s, supporting information), revealed a main effect of dose ($F_{(3,21)}$ = 4.30; $p < 0.05$), a main effect of test ($F_{(1,7)}$ = 24.4; $p < 0.01$) and a significant dose by test interaction ($F_{(3,21)}$ = 4.70; $p < 0.05$; Figure 2s). Post hoc analysis revealed a significant reinstatement effect following pretreatment with vehicle, 10 mg/kg of **3**, or 3.2 mg/kg of **3** (p < 0.05). With respect to the effect of **3** on reinstatement of fentanyl seeking, post hoc analysis revealed that **3** decreased active lever responses under reinstatement test conditions at 32 mg/kg compared to vehicle. Analysis of inactive lever responses failed to reveal a main effect of test, main effect of dose, or dose by interaction effect.

At this dose it is expected that both the D3R and D2R receptors will be highly occupied, so dual antagonism seems to be responsible for the observed activity. These results make a compelling case for D3R/D2R antagonism in both the cessation and relapse phase of opioid addiction treatment.

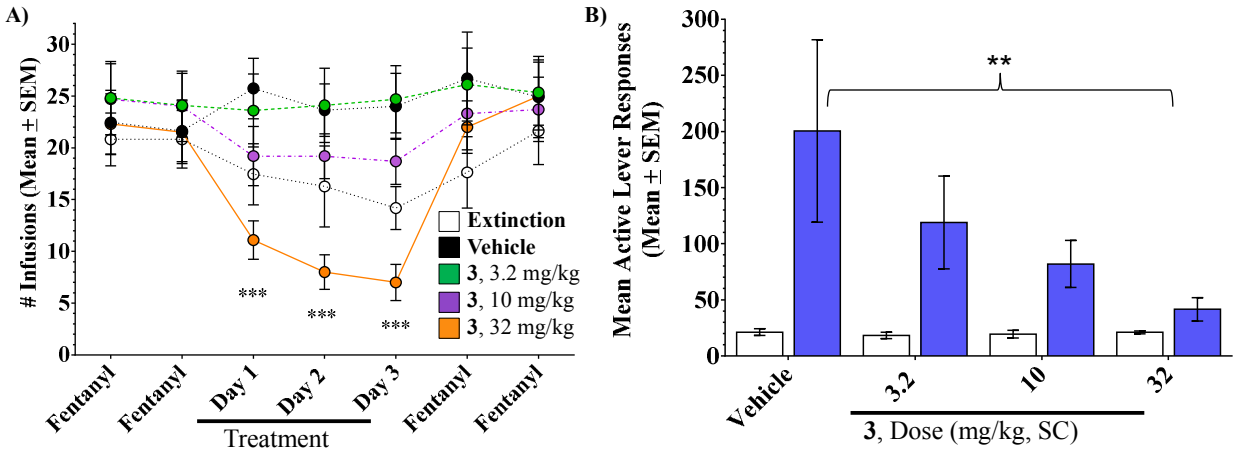

Figure 4. A) Effects of vehicle or **3** pretreatment on fentanyl self-administration over 3 test days in the rat model of cessation. Data represent the average infusions of fentanyl across baseline responding (fentanyl) before and after test sessions as well as three consecutive test sessions with **3** (Days 1–3). Saline extinction tests (Extinction) are also shown, in which saline was substituted for fentanyl during test sessions. n = 9–11; *** $p < 0.001$. B) Effects of **3** on combined cue and fentanyl prime-induced reinstatement of fentanyl-seeking behavior. Data represent mean ± SEM active lever responses, with white bars representing baseline active lever responses and blue bars representing active lever response on reinstatement test conditions. n = 8; ** $p < 0.01$

Conclusion

Via examination of compounds with D3R and D2R binding and functional data in our corporate compound file, we identified the unique structural scaffold **1**. Through a hybrid approach, we merged key pharmacophore elements from D3 antagonist **1** and D3 agonist **2** to

yield the novel D3R/D2R antagonist **3**. Compound **3** possessed CNS drug-like properties as defined by ADME attributes and CNS MPO desirability score (≥4/6).[36, 37] In addition to good physicochemical properties, **3** exhibited low nanomolar affinity for the D3R (D3 K_i = 3.1 nM) and good subtype selectivity over D2R (D2 K_i = 692 nM). The D3R functional potency of **3** was in line with its binding affinity, establishing **3** as an antagonist with a D3R functional K_i of 1.1 nM. Compound **3** exhibited excellent brain penetration in rats, with equivalent free drug levels in plasma and brain compartments ($C_{b,u}/C_{p,u}$ = 1). Given the higher-than-expected D2R occupancy in the ex vivo receptor occupancy assay, we were concerned that significant D2R side effects would be observed at low doses. When we examined **3** in models that evaluate D2R-associated liabilities, we were surprised to discover that high D2R occupancy (86% RO) did not result in either the locomotor or catalepsy side effects characteristic of traditional D2R antagonists such as haloperidol and eticlopride which induce catalepsy in rodents at D2R occupancies of >50%. While we do not fully understand why **3** was devoid of these side effects, one potential explanation is that very high D3R occupancy counters these responses to moderate D2 receptor blockade in specific neural pathways. An alternative explanation could be that **3** has a unique binding mode in either D3R or D2R that differentially modulates in vivo functional signaling, compared to traditional D2R antagonists. Recent reports[47, 48] suggest that D3/D2 dimerization is critical to the functional effects of D2R, allowing for the hypothesis that **3** is binding in a unique way to this heteromer complex and thus changing the downstream signaling events. Lastly, moderate affinity of **3** to 5HT2a could help explain the lack of locomotor or catalepsy side effects, however, other compounds from this series devoid of 5HT2a activity have similar in vivo profiles to **3**. Ongoing studies, including the generation of a crystal structure of **3** interacting with either D3R or D2R, may provide insight into this potential unique binding pose,

and single molecule fluorescence experiments could be used to determine if binding of **3** alters or prevents dimerization of dopamine receptors, thereby differentially modulating in vivo functional effects. Induced-fit docking[49] of **3** into the published D3R X-ray crystal structure (PDB ID: 3PBL)[50] suggests the possibility of two binding modes. Neither of these binding modes is fully predictive of the SAR and selectivity in this series, however, nor is it clear what could potentially disrupt D3/D2 dimerization from either of these binding poses; the true binding mode of **3** to D3R or D2R therefore remains unclear.

Compound **3** is well tolerated in animals at high D3R and D2R occupancy, allowing for the full examination of a range of both D3R and D2R occupancy of **3** on cessation of drug-taking and relapse to drug-seeking. The current study demonstrated a connection between D3R/D2R antagonism and attenuation of drug-seeking behavior, with compound **3** decreasing fentanyl self-administration (cessation) and robustly attenuating the reinstatement of fentanyl-seeking behavior under combined cue and prime conditions. Drug-seeking behavior can be characterized by the acquisition and maintenance of drug-taking behavior and the relapse to drug-seeking behavior, consisting of forced abstinence from drug-taking and a reinstatement/relapse event triggered by a drug prime or drug cue presentation (Figure 5). In the current model, the proposed efficacy of a D3/D2 receptor antagonist is highlighted by a potential benefit in both cessation of a drug-taking (as evidenced by the decrease in fentanyl self-administration) as well as a prevention of relapse (as evidenced by a decrease in fentanyl reinstatement) following pretreatment with compound **3**. Considering the increased efficacy observed following administration of 32 mg/kg relative to 10 mg/kg, the current results suggest that addition of D2R antagonism is beneficial in driving the efficacy of reducing drug-seeking behavior compared to D3R antagonism alone. A potential alternative interpretation of these results is that compound **3**

is inducing a non-specific effect on motor function or general motivation, resulting in decreased fentanyl self-administration and reinstatement, rather than specifically attenuating fentanyl-seeking. However, results from the current study demonstrate that compound **3** does not alter locomotor activity up to 32 mg/kg. Furthermore, the effect of compound **3** in an intracranial self-stimulation (ICSS) model designed to understand potential anhedonic effects of compounds revealed no change in ICSS behavior at efficacious doses, which suggests a specific effect on fentanyl-associated motivation.. Thus, given that the rat reinstatement model of drug relapse possesses high predictive validity for efficacy in substance use disorders,[51] these data suggest that dual D3/D2 receptor antagonists warrant further investigation in clinical studies examining both the drug cessation and relapse phases of substance use disorder treatment.

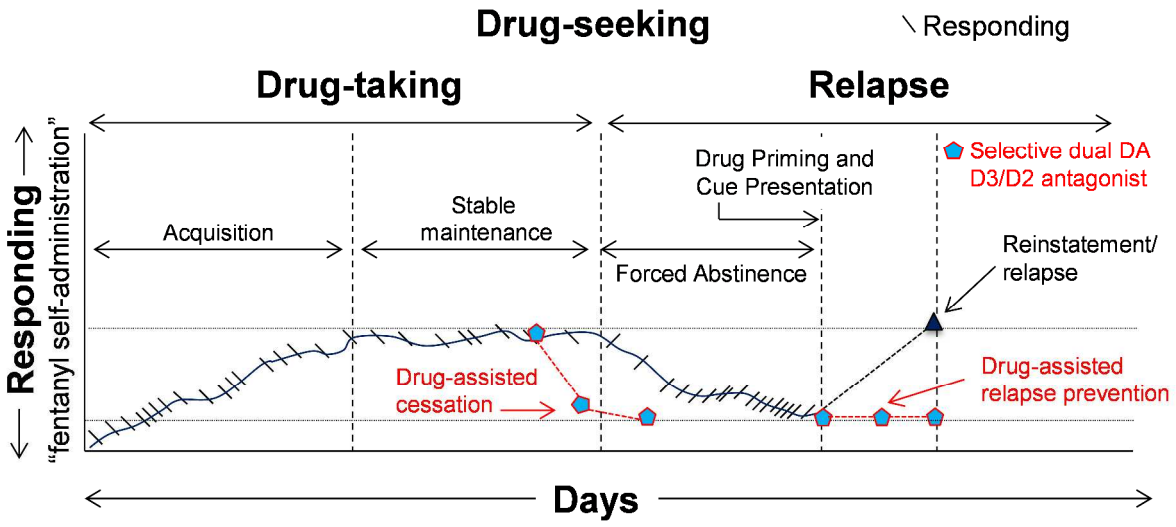

Figure 5. General depiction of the experiment. Selective D3/D2 antagonist **3** attenuates fentanyl-seeking behavior in models of both cessation of fentanyl self-administration and reinstatement (as a model of relapse).

In summary, compound **3** is an excellent preclinical tool to functionally probe the biology of D3R and D2R in vivo. While it does not meet our guidelines [$C_{eff} \leq 250$ nM (total

drug)] to move into preclinical in vivo safety testing,[52] the discovery of **3** is a significant advancement in the development of D3R/D2R antagonists for the treatment of drug addiction.[27] The unique in vivo profile of **3** makes it a promising candidate for preclinical testing of D3/D2 antagonism for multiple substance use disorders.

METHODS

Physicochemical Properties and Data Analysis. For the work herein, calculated CNS MPO desirability scores were obtained using the published algorithm,[37] and calculated physicochemical properties were obtained using standard commercial packages: Biobyte for ClogP calculations; for calculation of TPSA, see Ertl.[53] Statistical analyses were carried out using SigmaPlot version 11.0, from Systat Software, Inc., San Jose California USA, www.sigmaplot.com .

ADME Data. Data on the following in vitro ADME properties were obtained from the company database. All assays were performed via reported methods as described previously for: (a) passive apparent permeability, P_{app}, assay;[54] (b) P-glycoprotein (P-gp) efflux liability assay;[54] (c) metabolic stability, expressed as unbound intrinsic clearance ($CL_{int,u}$);[55, 56] and (d) plasma protein binding, F_u mouse and human.

Chemistry

The synthesis of **3** begins with commercially available starting materials, as illustrated in Scheme 1. Conversion of 3-methyl-4-nitrobenzoic acid (**4**) to the corresponding acid chloride with thionyl chloride and catalytic DMF gave 3-methyl-4-nitrobenzoyl chloride (**5**) in 91% crude yield (500 g). Treatment of crude **5** in acetonitrile/ THF with (trimethylsilyl)diazomethane generated the α-diazoketone in situ, which by addition of 40% aq. HBr was converted to 2-bromo-1-(3-methyl-4-nitrophenyl)ethanone (**6**) in 93% isolated yield (600 g). Morpholin-2-ol **7**

was prepared in 52% isolated yield (320 g) via bromide displacement of α-bromoketone **6** with 2-(ethylamino)ethanol and subsequent cyclization to the lactol. Hydrodehydroxylation of **7** with TFA/triethylsilane in CH_2Cl_2 yielded 4-ethyl-2-(3-methyl-4-nitrophenyl)morpholine (**8**) (200 g) in 66% isolated yield. Reduction of the nitro group in **8** to the corresponding amine was accomplished via Raney nickel hydrogenation in MeOH to give 4-(4-ethylmorpholin-2-yl)-2-methylaniline (**9**) in 63% isolated yield (110 g). Completing the sequence, racemic sulfonamide **10** was prepared in 99% isolated yield (20 g) by treatment of aniline **9** with commercially available 4-isopropylbenzene-1-sulfonyl chloride in pyridine. Preparative chiral chromatography of this sulfonamide, followed by HCl salt formation, afforded the enantiomerically pure title compound (-)-*N*-{4-[(2*S*)-4-ethylmorpholin-2-yl]-2-methylphenyl}-4-(propan-2-yl)benzenesulfonamide (**3**).

Scheme 1: Synthesis of D3R/D2R antagonist **3**.

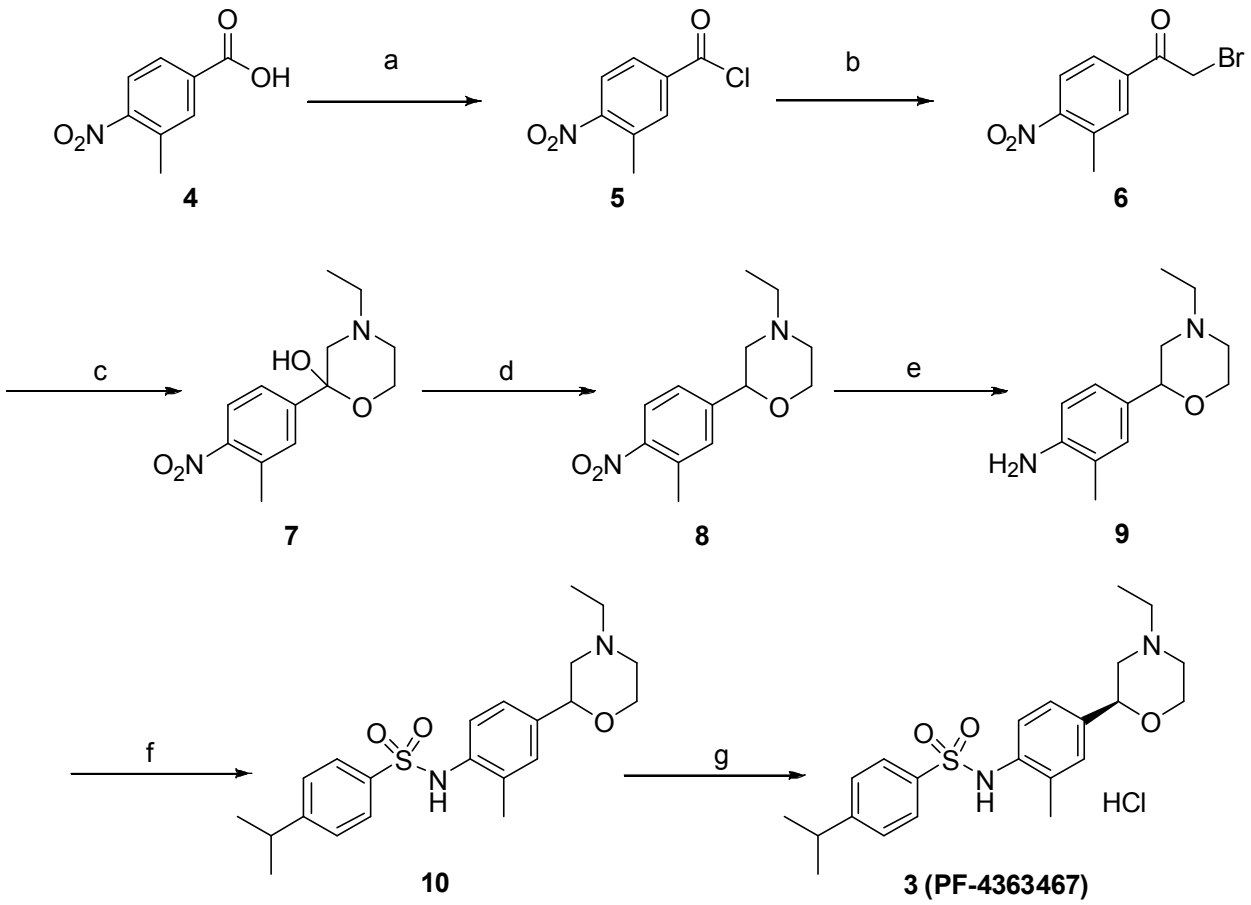

4 **5** **6** **7** **8** **9** **10** **3 (PF-4363467)**

Reagents and conditions: a) thionyl chloride, DMF; b) (trimethylsilyl)diazomethane, ACN/THF, then 40% HBr; c) 2-(ethylamino)ethanol, Et_3N, CH_2Cl_2; d) triethylsilane, TFA, CH_2Cl_2; e) H_2, Raney Ni, MeOH; f) 4-isopropylbenzene-1-sulfonyl chloride, pyridine; g) chiral chromatographic separation, then HCl/EtOAc/Et_2O.

Chemistry Experimental Section. General Information. All solvents and reagents were obtained from commercial sources and were used as received. All reactions were followed by TLC (TLC plates F254, Merck) or LCMS (liquid chromatography-mass spectrometry) analysis. Proton and ^{13}C NMR spectra were obtained using deuterated solvents on a Varian 400 MHz instrument. All proton shifts are reported in δ units (ppm) downfield of TMS (tetramethylsilane) and were measured relative to the signals for chloroform (7.27 ppm) and methanol (3.31 ppm).

All ^{13}C shifts are reported in δ units (ppm) relative to the signals for chloroform (77.0 ppm) and methanol (49.1 ppm) with ^{1}H-decoupled observation. NMR abbreviations are as follows: br, broadened; s, singlet; d, doublet; t, triplet; q, quartet; p, pentuplet; m, multiplet; dd, doublet of doublets; dddd, doublet of doublet of doublet of doublets; sept, septuplet; tt, triplet of triplets. Analytical analyses by UPLC were performed on a Waters Acquity system with PDA detection (UV 210 nm) at 45 ºC, flow rate 0.5 mL/min, with a 95/5 buffer/acetonitrile (0 to 7.55 min), 10/90 buffer/acetonitrile (7.55 to 7.85 min) using the following columns and buffers: Waters BEH C8 column (2.1 x 100 mm, 1.7 µm) with 50 mM sodium perchlorate/0.1% phosphoric acid or 10 mM ammonium bicarbonate as buffer; Waters BEH RP C18 column (2.1 x 100 mm, 1.7 µm) or Waters HSS T3 (2.1 x 100 mm, 1.8 µm) column with 0.1% methanesulfonic acid buffer. All melting points are uncorrected. Elemental analyses were performed by QTI Development. Mass spectra were recorded on a Micromass ADM atmospheric pressure chemical ionization instrument (MS, APCI). High resolution mass spectra were obtained on an Agilent LC-MS TOF equipped with a Zorbax Eclipse column (50 mm x 4.6 mm, 1.8 µm XDB-C18) using 0.1% aqueous formic acid as mobile phase A1 and acetonitrile containing 0.1% formic acid as mobile phase B1. Column chromatography was carried out on silica gel 60 (32–60 mesh, 60 Å) or on pre-packed Biotage™ columns. The purities of final compound **3** and **4–10** as measured by UPLC were found to be above 95%.

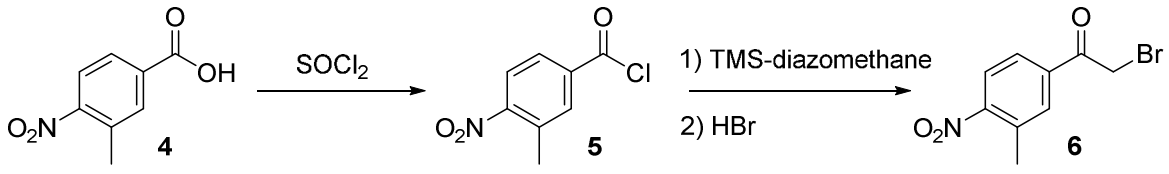

Preparation of 2-bromo-1-(3-methyl-4-nitrophenyl)ethanone (6). A mixture of 3-methyl-4-nitrobenzoic acid (**4**) (500.0 g, 2.8 mol), DMF (10 mL) and thionyl chloride (2.0 L, 26.8 mol) was refluxed for 10 h. The thionyl chloride was removed in vacuo and the residue was re-

concentrated from heptane three times to yield 3-methyl-4-nitrobenzoyl chloride (**5**) (500.0 g, 91%) as a brown oil which was used without purification. For analytical purposes, a portion of this material was recrystallized from heptane to give a light yellow solid: ^{1}H NMR (400 MHz, $CDCl_3$) δ ppm 8.05 - 8.08 (m, 2H), 7.98 (d, *J* = 8.8 Hz, 1H), 2.63 (s, 3H). The crude acid chloride (500.0 g, 2.5 mol) was dissolved in CH_3CN/THF (1:1, 8.0 L) and cooled to 0 ºC. A solution of 2 M (trimethylsilyl)diazomethane in hexanes (1.5 L, 3.0 mol) was added drop-wise. The resulting mixture was warmed to rt and stirred for 1 h. The reaction was re-cooled to 0 ºC and 40% aq. HBr (1.0 kg, 5.0 mol) was added drop-wise. After stirring at rt for 30 min, the reaction was concentrated in vacuo to yield 2-bromo-1-(3-methyl-4-nitrophenyl)ethanone (**6**) (600.0 g, 93.0%) as a brown solid. ^{1}H NMR (400 MHz, $CDCl_3$) δ ppm 7.89 - 8.05 (m, 3H), 4.45 (s, 2H), 2.66 (s, 3H); ^{13}C NMR (100 MHz, $CDCl_3$) δ ppm 190.2, 152.3, 137.0, 134.2, 133.5, 127.6, 125.2, 30.5, 20.3; HRMS *m/z* (+TOF) $[M + H]^+$ calcd. for $C_9H_8NO_3S$, 257.9760; found, 257.9753.

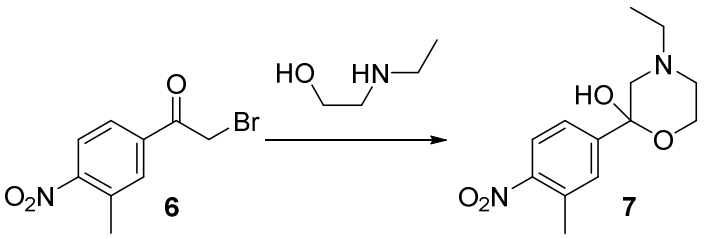

Preparation of 4-ethyl-2-(3-methyl-4-nitrophenyl)morpholin-2-ol (7). 2-Bromo-1-(3-methyl-4-nitrophenyl)ethanone (**6**) (600.0 g, 2.3 mol), 2-(ethylamino)ethanol (228 mL, 2.6 mol) and Et_3N (259 g, 2.6 mol) in dichloromethane (3.5 L) were stirred at rt for 16 h. The reaction mixture was washed with brine (1.5 L), and the aqueous layer was extracted with ethyl acetate (3×3 L). The combined organic layers were dried over $MgSO_4$ and concentrated. The residue was purified by silica gel chromatography (pet. ether/EtOAc 10:1) to give 4-ethyl-2-(3-methyl-4-nitrophenyl)morpholin-2-ol (**7**) (320 g, 52.0%) as a brown oil. ^{1}H NMR (400 MHz, $CDCl_3$) δ

ppm 7.96 (d, *J* = 8.4 Hz, 1H), 7.57 - 7.64 (m, 2H), 4.95 (br s, 1H), 4.18 (ddd, *J* = 11.9, 11.9, 2.9 Hz, 1H), 3.86 (dd, *J* = 11.6, 3.6 Hz, 1H), 2.76 - 2.85 (m, 2H), 2.61 (s, 3H), 2.41 - 2.53 (m, 2H), 2.32 (ddd, *J* = 11.7, 11.7, 3.8 Hz, 1H), 2.19 (d, *J* = 10.9 Hz, 1H), 1.09 (t, *J* = 7.2 Hz, 3H); ^{13}C NMR (100 MHz, $CDCl_3$) δ ppm 149.1, 147.0, 133.6, 130.6, 124.8, 94.4, 63.4, 60.9, 52.3, 52.0, 20.8, 11.9; HRMS *m/z* (+TOF) $[M + H]^+$ calcd. for $C_{13}H_{18}N_2O_4$, 267.1339; found, 267.1331.

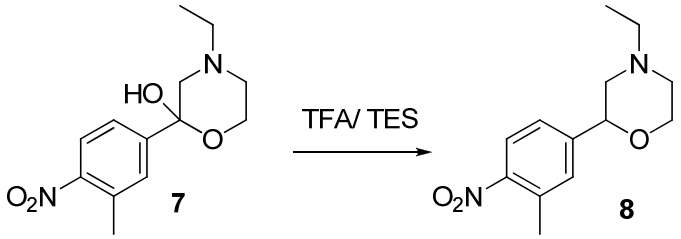

Preparation of 4-ethyl-2-(3-methyl-4-nitrophenyl)morpholine (8). A mixture of 4-ethyl-2-(3-methyl-4-nitrophenyl)morpholin-2-ol (**7**) (320 g, 1.2 mol), triethylsilane (720 mL, 6.0 mol) and TFA (3.2 L) in CH_2Cl_2 (6.0 L) was stirred at rt for 72 h. Saturated aq. K_2CO_3 was added until the pH was 10. The organic layer was separated and the aqueous layer was extracted with ethyl acetate (3x1.5 L). The combined organic layers were dried over $MgSO_4$ and concentrated, and the residue was purified by silica gel chromatography (petroleum ether) to yield 4-ethyl-2-(3-methyl-4-nitrophenyl)morpholine (**8**) (200 g, 66.0%) as a brown oil. This material was suitable for use without further purification. For analytical purposes, a portion was converted to the hydrochloride salt and recrystallized from $CHCl_3$/ EtOAc, yielding a light orange-tinged solid: ^{1}H NMR (400 MHz, $CDCl_3$) δ ppm 13.54 (br s, 1H), 7.99 (d, *J* = 8.6 Hz, 1H), 7.36 - 7.42 (m, 2H), 5.44 (d, *J* = 9.4 Hz, 1H), 4.53 - 4.61 (m, 1H), 4.23 (dd, *J* = 13.1, 3.1 Hz, 1H), 3.57 (t, *J* = 10.9 Hz, 2H), 3.10 - 3.18 (m, 2H), 2.86 - 2.98 (m, 1H), 2.56 - 2.65 (m, 4H), 1.54 (t, *J* = 7.2 Hz, 3H); ^{13}C NMR (100 MHz, $CDCl_3$) δ ppm 149.2, 141.8, 134.3, 130.3, 125.3, 124.3, 73.8, 63.6, 56.2, 52.9, 50.4, 20.4, 8.9; HRMS *m/z* (+TOF) $[M + H]^+$ calcd. for $C_{13}H_{18}N_2O_3$, 251.1390; found, 251.1387.

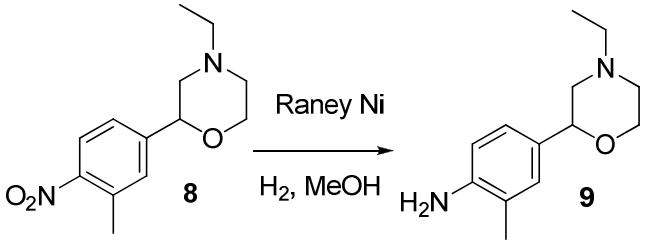

Preparation of 4-(4-ethylmorpholin-2-yl)-2-methylaniline (9). A mixture of 4-ethyl-2-(3-methyl-4-nitrophenyl)morpholine (**8**) (200 g, 0.80 mol) and Raney nickel (20 g) in MeOH (5.0 L) was stirred under 1 atm of H_2 at rt for 24 h. The mixture was filtered and washed with MeOH (3x100 mL). The filtrate was concentrated and the residue was purified by chromatography on silica gel (petroleum ether/EtOAc 5:1) to give 4-(4-ethylmorpholin-2-yl)-2-methylaniline (**9**) (110 g, 62%) as a brown oil: ^{1}H NMR (400 MHz, $CDCl_3$) δ ppm 7.07 (s, 1H), 7.03 (dd, *J* = 8.1, 1.9 Hz, 1H), 6.64 (d, *J* = 8.0 Hz, 1H), 4.45 (dd, *J* = 10.4, 2.3 Hz, 1H), 4.02 (ddd, *J* = 11.4, 3.4, 1.4 Hz, 1H), 3.83 (ddd, *J* = 11.5, 11.5, 2.3 Hz, 1H), 3.59 (br s, 2H), 2.91 (ddd, *J* = 11.5, 2.0, 2.0 Hz, 1H), 2.81 (dd, *J* = 11.3, 1.8 Hz, 1H), 2.45 (q, *J* = 7.1 Hz, 2H), 2.15 - 2.23 (m, 4H), 2.05 (dd, *J* = 11.4, 10.4 Hz, 1H), 1.11 (t, *J* = 7.2 Hz, 3H); ^{13}C NMR (100 MHz, $CDCl_3$) δ ppm 144.5, 130.8, 128.7, 125.3, 122.4, 114.9, 78.5, 67.4, 60.5, 52.9, 52.8, 17.6, 12.0; HRMS *m/z* (+TOF) $[M + H]^+$ calcd for $C_{13}H_{20}N_2O$; 221.1648, found, 221.1646.

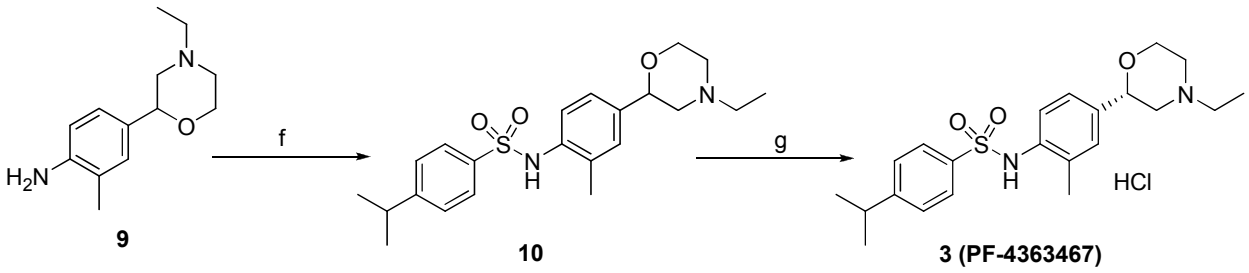

Preparation of (-)-*N*-{4-[(2*S*)-4-ethylmorpholin-2-yl]-2-methylphenyl}-4-(propan-2-yl)benzenesulfonamide (3). 4-Isopropylbenzene-1-sulfonyl chloride (8.9 mL, 49.9 mmol) was added to an ice cooled solution of 4-(4-ethylmorpholin-2-yl)-2-methylaniline (**9**) (11.0 g, 49.9

mmol) in pyridine (106 mL) and the resulting reaction mixture was slowly warmed to rt. After stirring overnight, the reaction was concentrated and the residual oil was dissolved in CH_2Cl_2 and washed with 1 N NaOH, dried over $MgSO_4$, and concentrated to yield 28 g of crude *N*-[4-(4-ethylmorpholin-2-yl)-2-methylphenyl]-4-(propan-2-yl)benzenesulfonamide. Chromatography on a 350 g ISCO cartridge using EtOAc and 5% EtOH / EtOAc gave 20 g (>99%) of purified material as an amorphous glass: ^{1}H NMR ($CDCl_3$) δ 7.66 (d, *J* = 8.5 Hz, 2H), 7.28 - 7.23 (m, 3H), 7.12 - 7.08 (m, 2H), 4.49 (dd, *J* = 10.3, 1.9 Hz, 1H), 4.5 - 3.95 (m, 1H), 3.82 (ddd, *J* = 11.6, 11.2, 2.5 Hz, 1H), 2.94 - 2.78 (m, 3H), 2.50 - 2.42 (m, 2H), 2.24 - 2.15 (m, 1H), 2.02 - 1.96 (m, 1H), 1.97 (s, 3H), 1.26 - 1.20 (m, 6H), 1.05 (t, *J* = 9.5 Hz, 3H); ^{13}C NMR ($CDCl_3$) δ 154.7, 138.4, 134.2, 131.6, 129.2, 128.7, 127.5, 127.3, 125.0, 124.4, 67.3, 60.2, 52.8, 52.7, 34.5, 34.3, 23.8, 17.8, 11.8; LRMS *m/z* calcd for $C_{22}H_{30}N_2O_3S$, 402.56; found, 403.3 $[M + H]^+$, (APCI); R_f = 0.4 (10% EtOH / EtOAc). The enantiomers of *N*-[4-(4-ethylmorpholin-2-yl)-2-methylphenyl]-4-(propan-2-yl)benzenesulfonamide were separated by preparative chiral chromatography (10 cm x 50 cm Chiralpak AD column using 75/25 heptane/EtOH as mobile phase with a flow rate of 500 mL/ min) to yield 7.7 g of enantiomer #1 (**3**, r.t. = 8.49 min; $[\alpha]_D = -3.025$, c = 1.20 in MeOH) and 7.7 g of enantiomer #2 (PF-04363476; r.t. 13.43 min). The HCl salt of enantiomer #1 (**3**) was prepared in EtOAc (150 mL) by adding 1 eq. of 2 N HCl/ether followed by ether (150 mL). The resulting slurry was stirred overnight, filtered, dried under N_2 and evacuated overnight to yield 7.7 g of the mono HCl salt of **3** as a light yellow-tinted solid: mp = 218–220 ºC; ^{1}H NMR (400 MHz, $CDCl_3$) δ ppm 13.05 (br s, 1H), 7.67 (d, *J* = 8.4 Hz, 2H), 7.28 - 7.30 (m, 3H), 7.10 - 7.12 (m, 2H), 7.06 (s, 1H), 5.20 (dd, *J* = 10.7, 1.6 Hz, 1H), 4.45 - 4.54 (m, 1H), 4.15 (dd, *J* = 13.0, 3.4 Hz, 1H), 3.48 - 3.56 (m, 2H), 3.09 - 3.17 (m, 2H), 2.83 - 2.99 (m, 2H), 2.60 - 2.68 (m, 1H), 2.03 (s, 3H), 1.50 (t, *J* = 7.3 Hz, 3H), 1.24 (d, *J* = 6.9 Hz, 6H); ^{13}C NMR (100 MHz,

$CDCl_3$) δ 154.7, 137.0, 135.3, 134.3, 132.1, 128.7, 127.2, 127.1, 124.5, 124.4, 74.4, 63.6, 56.3, 52.8, 50.5, 34.1, 23.6, 17.7, 8.8; Anal. calcd. for $C_{22}H_{30}N_2O_3S$•HCl: C, 60.19; H, 7.12; N, 6.38; Found: C, 60.32; H, 7.37, N, 6.26. The absolute stereochemistry was determined using small molecule crystallography. Pertinent crystal, data collection and refinement information is summarized in the small molecule report, supplementary material.

In vitro Materials.

Binding Assay.

Binding assays were performed using over-expressing human D2 and D3 CHO cell lines. To determine basic assay parameters, ligand concentrations were determined from saturation binding studies, where the K_d using [^{3}H]-spiperone (PerkinElmer NET1187250UC) for D2 binding was determined to be 1.6 nM and a K_d of 1.4 nM was determined for hD3 using [^{3}H]-7-OH-DPAT (PerkinElmer NET1169250UC). From tissue concentration curve studies, the optimal amount of tissue was determined to be 4 mg/mL for hD2 and 7 mg/mL for hD3 per 96-well plate. These ligand and tissue concentrations were used in time-course studies to determine linearity and equilibrium conditions for binding. It was found that binding was at equilibrium with the specified amount of tissue in 20 minutes at 37 °C for both receptors. From these parameters, K_i values were determined by homogenizing the specified amount of tissue for each receptor in 50 mM Tris (pH 7.4 at 4 °C) containing 2.0 mM $MgCl_2$, and spinning in a centrifuge at 40,000 x *g* for 10 minutes. The pellet was resuspended in either the D2 assay buffer [50 mM Tris (pH 7.4 @ 37 °C), 100 mM NaCl and 1 mM $MgCl_2$] or the D3 assay buffer [50 mM Tris (pH 7.4 at 37 °C), 120 mM NaCl, 5 mM $MgCl_2$, 5 mM KCl and 2 mM $CaCl_2$]. Incubations were initiated by the addition of 200 µL of tissue to 96-well plates containing test drugs (2.5 µL) and 1.6 nM [^{3}H]-spiperone for D2 or 1.5 nM of [^{3}H]-7-OH-DPAT for D3 (both 50 µL) for a final

assay volume of 250 μL. Non-specific binding was determined by radioligand binding in the presence of a saturating concentration of haloperidol. After the 20 minute incubation period at 37 °C, assay samples were rapidly filtered through Unifilter-96 GF/B PEI-coated filter plates and rinsed with ice-cold 50 mM Tris buffer (pH 7.4 at 4 °C). Membrane radioligand levels were determined by liquid scintillation counting of the filter plates in 50 μL EcoLume. The IC_{50} value (concentration at which 50% inhibition of specific binding occurs) was calculated by linear regression of the concentration-response data in Activity Base (IDBS). K_i values were calculated according to the Cheng-Prusoff equation.

D2 Functional Assay. cAMP Accumulation Assay in SH-SY5Y hD2L Cells:

Human D2L-transfected SH-SY5Y cells were grown at 37 °C and 5% CO_2 in DMEM/F12 medium supplemented with 10% dialyzed FBS and 100 μg/mL G418. The cells were frozen as assay-ready vials and thawed immediately prior to the assay. On the day of the experiment, compounds dissolved in DMSO were diluted in pH 7.4 assay buffer containing PBS, 5 μM HEPES, and 100 μM IBMX (final concentrations). The vial of frozen cells was rapidly thawed in a 37 °C water bath. Cells were washed with PBS and centrifuged to obtain a pellet. The pellet was resuspended in warm PBS and the cells were allowed to sit for 5 minutes, prior to counting and dilution. The reaction was initiated by addition of the cells into 384-well plates containing test compounds; the final number of cells used in the assay was 10000–15000 cells per well. Cells and compounds were pre-incubated together for 10 minutes at 37 °C. NKH477 was then added to the plates at a final concentration of 3 μM to activate adenylyl cyclase and increase basal levels of cAMP. For testing compounds in agonist mode, assay buffer was added to the plate; in antagonist mode, a D2 agonist was added to produce an 80% agonist effect (quinelorane, 32 nM). Plates were then returned to the 37 °C incubator and incubated for 15

minutes at 37 °C. To stop the reaction, Cisbio cAMP Dynamic 2 screening kit reagents (cat# 62AM4PEB) were added to the plate. Homogenous time-resolved fluorescence-based cAMP (Schering) detection was determined according to the manufacturer's instruction. A Wallac EnVision was used to measure HTRF (excitation 320 nm, emission 665 nm/620 nm, delay time 50 μs, window time 400 μs). Data was analyzed based on the ratio of fluorescence intensity of each well at 620 nm and 665 nm followed by cAMP quantification using a cAMP standard curve. Agonist activity of a compound was measured by its ability to decrease the cAMP production elicited by NKH477. The agonist effect was normalized to the % effect of 1 μM quinelorane. Antagonist activity was measured by a compound's ability to reverse the agonist-induced decrease of cAMP (in the presence of NHK477). The antagonist effect was normalized to the % effect of NHK477 alone.

D3 Functional Assay. GTP-γ-S Binding Assay in SH-SY5Y hD3 Cells: SH-SY5Y hD3 cells were grown at 37 °C and 5% CO2 in DMEM/F12 supplemented with 10% dialyzed FBS and 100 μg/mL G418. Cell paste was frozen in a pellet and stored at −80 °C until ready for use. The day of the assay, cell paste was homogenized using a glass-Teflon homogenizer in buffer containing 50 mM HEPES, 1 mM EDTA and protease inhibitors (pH 7.4, 4 °C). The membranes were centrifuged at 40000 x *g* for 10 minutes. The pellet was resuspended in pH 7.4 assay buffer (20 mM HEPES, 100 mM NaCl, 30 mM $MgCl_2$). Saponin and guanosine diphosphate (44 μg/mL and 30 μM final assay concentrations, respectively) were added to the membrane solution. The membranes were incubated at 4 °C for 1 hour to promote GDP binding. Membranes were then added to test compounds (in DMSO) in the assay plate and incubated for 30 minutes at 30 °C. [^{35}S] GTP-γ-S was added to the assay plate (final assay concentration of 1 nM) and incubated another 30 minutes at 30 °C. To stop the reaction, assay samples were rapidly filtered through

GF/B fired UniFilter plates (PerkinElmer) and rinsed with ice-cold 50 mM Tris buffer (pH 7.4). Filter plates were allowed to dry overnight. The next day, membrane-bound [^{35}S] GTP-γ-S levels were determined by liquid scintillation counting of the filter plates in EcoLume scintillation fluid. A background control of 10 μM cold guanosine triphosphate was subtracted from raw assay data prior to data analysis. Percent effect in the agonist assay was calculated by normalizing compound concentration data to 1 μM quinelorane (full agonist). Activity in the antagonist assay was determined by a compound's ability to reverse an 80% agonist effect (10 nM quinelorane). Percent effect in the antagonist assay was calculated by normalizing data back to basal levels of [^{35}S] GTP-γ-S binding. IC_{50} values (concentration at which 50% inhibition of specific binding occurs) were calculated by curve-fitting of the concentration-response data.

Ex Vivo Methods and Materials; Receptor Occupancy.

Frozen −80 ^{o}C male Sprague Dawley rat brain slices (20 μm) on gelatin-coated slides were thawed in a humidified chamber at 37 ^{o}C for 15 min and subsequently incubated for 15 min at room temperature with 0.3 nM [^{125}I]iodosulpiride in buffer (50 mM Tris-HCl, 120 mM NaCl, 5 mM KCl, 2 mM $CaCl_2$, 1 mM $MgCl_2$, 1 mM L-ascorbic acid pH 7.4). The reaction was stopped by 2 min rinses (2x) in cold buffer followed by a 30 second rinse in 4 ^{o}C deionized water. Slices were air-dried for 15 to 20 min under a stream of cool air and further dried for 30 min at room temperature under vacuum in a desiccant-containing vacuum bell. Dried slices were placed in x-ray cassettes and exposed to hyperfilm (Kodak BioMax MR) for 5 days with cerebellum slices for D3 quantitation or 36 hours with dorsal striatum slices for D2 quantitation. Specific binding was determined by calculation of total binding minus non-specific binding observed in the presence of 1 μM haloperidol. Images were semi-quantitatively evaluated using standard curves generated with [^{14}C]microscales.

In Vivo Methods and Materials: Effects of Administration of Compound 3 on Locomotor Activity and Catalepsy.

General Experimental. This study took place over 6 days with 8 animals tested each day. Locomotor activity was monitored for 3 hours, with catalepsy measurements taken at the beginning of each experiment and then at 30 minutes, 1 hour, 2 hours and 3 hours.

Animals and Conditions. Male Sprague Dawley rats (220–260 g) from Charles River were pair-housed with free access to water and food. Standard light/dark (0600 h/1800 h), temperature & humidity conditions were controlled and monitored.

Drugs. Compound **3** was dissolved in 10% 2-hydroxypropyl-beta-cyclodextrin at concentrations of 1.0, 3.2, 10.0 and 32.0 mg/mL, and dosed at 1.0, 3.2, 10.0 and 32.0 mg/kg. Haloperidol (Sigma) was dissolved in 1% acetic acid. The vehicle group received the same 10% 2-hydroxypropyl-beta-cyclodextrin that was used for dissolution of **3**. The route of administration was s.c., with an injection volume of 1.0 mL/kg; the pretreatment time was zero. All drug concentrations and doses refer to the active moiety.

Spontaneous Locomotor Activity Procedure/Chamber Apparatus. Procedure: Animals were brought in their home cages into the procedural room at least 30 minutes prior to testing and allowed to acclimate to the test room. Animals were assigned to treatment groups and locomotor boxes. On days 1–6, animals (1–2 per treatment group) were given a baseline catalepsy assessment, then given a s.c. injection of vehicle or drug and placed in Amlogger locomotor monitoring equipment for three hours of activity monitoring. Dependent measures included total activity and total distance travelled.

Inside the Amlogger equipment the rat was placed in a rat-sized housing box with a microisolator top located within a Linton Instrumentation (Norfolk, England) AM548 / AM524

IR Locomotor Activity Monitor. Three hours of activity were monitored by 24 infrared beams arranged in an 8 x 16, 1" (25.4 mm) pitched grid. Data were reduced by AMON Control and Data Logging Windows Software. The AMON software runs on Windows PCs, and was used to configure the experimental protocol and record activity data via a standard RS232 serial port. The AMON software discriminates between different types and speeds of movement. As such, the data that were logged provide a detailed breakdown of the various categories of activity. This software has the ability to start cages independently of one another and to review files during and after data acquisition. Data were output to an Excel spreadsheet. The software includes a self-test utility which verifies that all IR beams are functioning correctly.

Catalepsy Testing. Apparatus and procedure: Rats from the spontaneous locomotor activity procedure were used. At 0 (pre-injection) 30, 60, 120, 180 min after injection, the rats were removed from the Amlogger equipment and tested for catalepsy. Testing was accomplished by placing each rat in an upright position with its forepaws resting on a horizontal bar (9 mm in diameter) suspended at a height of 10 cm; the latency to removal of forepaws and reversion to a "normal" position was recorded. The maximum time limit was set at 90 seconds. After assessment of catalepsy, the rats were returned to the Amlogger equipment and activity was monitored until the next catalepsy measurement, over a total of 3 hours of testing.

Data Analysis. Data from 6 groups of 8 rats were collected and analyzed by calculating the total activity for each parameter, in selected time periods of testing. Locomotor comparisons were made through multiple unpaired t-tests with a significance level set at 95%, and corrected for multiple comparisons using the Holm-Sidak method for each dose against vehicle at each time block. Catalepsy comparisons were made through a repeated measures ANOVA test with a significance level set at 95% and followed by a Dunnett's post-test.

In Vivo Methods and Materials: Effects of Administration of Compound 3 on Prolactin Release.

Animals. Sprague Dawley rats from Charles River (225–250 grams at delivery) were pair-housed in vent-rack cages and allowed free access to food and water. They were maintained on a 12 hour light/dark (0600 h/1800 h) cycle in environmentally controlled quarters. Rats were given one week to acclimate to the conditions prior to study initiation.

Tissue Harvest. Rats were habituated to the room 60 minutes prior to dosing. Subjects were dosed in 1 mL/kg volumes with **3** (0.1, 1.0, 10 mg/kg; s.c.), corrected for the weight of the salt or vehicle one hour prior to trunk blood collection. Trunk blood was obtained via decapitation without anesthesia and stored in EDTA-containing tubes from Becton, Dickinson and Company. Blood was spun down at 4000 RPM for 5 minutes. Plasma was stored at −20 °C.

ELISA. ELISA kits were purchased from ALPCO (Product number 55-PRLRT-E01) and the kit directions were precisely followed except that the standard curve was extended down to 0.625 ng/mL. Standards and individual subject plasma samples were run in duplicate. Plates were washed on an EL 406 washer dispenser (BioTek) and read on a SpectraMax Plus (Molecular Devices) using SoftMax Pro 4.8 software.

Data Analysis. Data were organized in Excel and the standard curve was calculated using GraphPad ver. 6 software. Individual concentrations were interpolated from this curve using GraphPad. Groups were compared and p-values were calculated within GraphPad using a one-way ANOVA. The ANOVA revealed significantly different standard deviations; therefore the data were logarithmically (base 10) transformed within GraphPad with the equation [y=log(y)]. Data were then compared using a one-way ANOVA followed by a Dunnett's post-test with a significance value of 0.05.

In Vivo Methods and Materials: Effects of Administration of (3) on cessation of fentanyl self-administration and reinstatement of fentanyl seeking.

Drugs. Fentanyl citrate salt (Sigma-Aldrich, St. Louis, MO) was dissolved in 0.9% saline solution. Compound **3** was formulated in 10% (2-hydroxypropyl)-beta-cyclodextrin (HPβCD). All drug concentrations and doses refer to the active moiety.

Surgery. Sprague Dawley rats (Charles River Laboratories, North Carolina, USA) were implanted with jugular vein catheters (JVC) with modifications to previously described methods.[57] Briefly, on the day of surgery, anti-inflammatory and antibiotic treatment was provided (carprofen: 5 mg/kg and enrofloxacin: 2.25 mg/kg; s.c.). After the rats had been anaesthetised with isoflurane (2.5–3.5% in 100% oxygen), a JVC (modified IVSAp40 catheter: CamCaths, Cambridge, UK), previously sterilized by exposure to ethylene oxide gas, was implanted. The proximal end was placed at the right atrium, entering at the right jugular vein, while the distal end was passed over the right shoulder and exited dorsally, between the scapulae. Carprofen (5 mg/kg) and enrofloxacin (2.25 mg/kg) were given subcutaneously for at least two days post-operatively. A minimum of seven days of postsurgical recovery was allowed prior to animal use in experiments. Catheter patency was maintained with daily iv infusions of 0.1 mL heparinized (50 units/mL) sterile 0.9% saline. During training and cessation self-administration sessions, animals were flushed daily with approximately 50 μL heparinized saline (50 U/mL) containing gentamicin (0.1 mg/mL). When rats were not used for periods longer than 48 hr, catheters were locked with approximately 50 μL of heparinized dextrose (100 U/mL) containing gentamicin (0.1 mg/mL). Catheter patency was assessed by injection of 0.1 mL propofol. Rats were food-restricted to ~22 grams of rodent diet per day, and fed at the end of each day after operant sessions had completed.

Apparatus. Self-administration training and testing occurred in operant chambers (ENV-008CT; Med-Associates, Vermont, USA) individually located within sound-attenuating cubicles, which were ventilated by an exhaust fan that also served to mask external noise. Two retractable response levers (ENV-112CM, Med-Associates) were located on one wall of the operant chamber, 12 cm apart and 6 cm from the grid floor. A cue light (ENV-221M, Med-Associates) was located approximately 4 cm above each lever. On the wall opposite to the response levers was positioned a house light (ENV-215M, Med-Associates) and response feedback clicker module (ENV-135M). Drug was infused by a fixed-rate syringe pump (PHM100, Med-Associates) located outside the sound-attenuating cubicle, via plastic tubing (polyethylene, SAI Infusion Technologies, Illinois, USA) connected from the infusion syringe to a stainless steel single-channel swivel (Model 375/22: Instech Laboratories, Pennsylvania, USA) mounted directly above the operant chamber on a counterbalanced lever arm (PHM-110, Med-Associates). A further length of tubing, shielded by a metal spring tether, connected the swivel to the external guide cannula of the implanted JVC. Med-PC IV software (Med-Associates) was used to control operant chambers and record data.

Self-administration Training Procedure. Self-administration, cessation and reinstatement methods were adapted from.[57] Rats were placed into the operant chambers and self-administration sessions commenced with an automatic infusion designed to fill the JVC with drug. The house light was then illuminated and both response levers were extended into the operant chamber. Responding on one lever (the active lever) under a fixed ratio schedule resulted in fentanyl delivery, followed by a timeout period of 20 seconds, during which time the cue lights located above the levers were flashed at a rate of 0.5 Hz and a clicking sound was presented at the same time as the light cue. Further responding during this timeout period on the

active lever was recorded but had no scheduled consequence. Responding on the alternative lever (the inactive lever) was recorded throughout the experimental session but had no scheduled outcome. Active and inactive levers were randomly assigned to each rat prior to the first session and did not change throughout the study. The unit dose of drug available was determined by the unit volume per infusion (as determined by the duration of the infusion) and adjusted for the weight of the rat. The duration of infusion was maintained at between 1 and 3 seconds. All experiments started between 8:00 AM and 3:00 PM, up to five days per week. All sessions were 1.5 hrs in duration.

Effects of Compound 3 on Cessation of Fentanyl Self-administration. Eleven rats were trained to respond for fentanyl (1 μg/kg/infusion) under an FR5 schedule of reinforcement (i.e., five responses on the active lever resulted in a single infusion of fentanyl). When rats were demonstrating stable self-administration of fentanyl under an FR5 schedule (as defined by ≤ 20% variation in the number of infusions obtained during two consecutive sessions), fentanyl was replaced with saline to extinguish responding. Following a minimum of three extinction sessions and demonstration of a reduction of 50% of the number of infusions received during the last two days of fentanyl self-administration behavior, rats were given the opportunity to reacquire fentanyl self-administration (1 μg/kg/infusion) and once stability criteria were achieved, the effect of **3** (0, 3.2, 10, and 32 mg/kg, s.c.) on fentanyl self-administration was assessed following a 30 min pretreatment prior to three consecutive fentanyl self-administration sessions. Following each three-session assessment of **3**, rats were given the opportunity to self-administer fentanyl for a minimum of two sessions until stability criteria were achieved before moving to the next dose. Included in the dose response was an additional saline extinction group, where saline was substituted for fentanyl during test sessions.

Effects of Compound 3 on Reinstatement of Fentanyl-seeking Behavior. Eight rats were trained to respond for fentanyl (1 μg/kg/infusion) under an FR5 schedule of reinforcement (i.e., five responses on the active lever resulted in a single infusion of fentanyl). When rats were demonstrating stable self-administration of fentanyl under an FR5 schedule (as defined by ≤ 20% variation in the number of infusions obtained during two consecutive sessions), responding was extinguished by removing the contingency between the response and fentanyl delivery. In addition, cues associated with the infusion were also removed, including the flashing cue lights, clicking sound, and the sound of the syringe pump. Following a minimum of five extinction sessions, and the demonstration of extinction (defined as a decrease in active lever responses to <20% of the mean number of responses made during the final two sessions of fentanyl responding), reinstatement sessions began. During a reinstatement test session, responses on the active lever resulted in delivery of the fentanyl-associated cues for 6 seconds; however, no fentanyl infusion was administered. Following each reinstatement session, rats were given extinction sessions until a minimum of 2 sessions met stability criteria, prior to the next reinstatement test session. To determine the effect of **3** on reinstatement of fentanyl-seeking behavior, doses of 0, 3.2, 10, and 32 mg/kg were administered. Compound **3** was given 30 minutes prior to all reinstatement tests. The order dose presentation of **3** was randomized.

Analysis. For the cessation tests, the dependent variable for statistical analyses was the number of drug infusions. The effects of **3** on fentanyl self-administration were analyzed using two-way repeated measures analysis of variance (ANOVA), with dose and session as factors. To permit direct comparison with baseline data, the baseline sessions preceding and following the test sessions were included in the analysis alongside the three test sessions for each dose condition. When a significant interaction was observed, comparisons on fentanyl self-administration were

performed between the **3** conditions and vehicle condition using one-way ANOVA followed by a Dunnett's post hoc test for each session. To understand the dose-response relationship, the average numbers of infusions obtained over all three test sessions were compared using a one-way ANOVA followed by a Dunnett's post hoc test.

For reinstatement tests, the baseline was defined as the average response on the two days preceding a reinstatement test, while the test was the number of responses on the reinstatement test session. Data from animals that did not reinstate under vehicle conditions, (i.e., exhibited fewer active lever presses on test compared to baseline) and outliers, (i.e., exhibited active lever presses greater than three standard deviations of the mean on vehicle) were excluded for each reinstatement condition.

For reinstatement tests, statistical analysis was performed using two-way repeated measures ANOVA, with session (baseline vs. test) and dose as factors for comparing responses (active and inactive lever presses) at baseline (i.e., the average of response rates during the sessions immediately preceding reinstatement sessions) with those during test reinstatement sessions. If a significant interaction or main-effect of dose was then observed, post hoc comparisons were made between responses following each dose of drug and vehicle, using Dunnett's test.

The significance level for all statistical tests was set at 0.05. All statistical analysis was performed using Statistica version 12.0 (StatSoft, Inc. 2014; STATISTICA (data analysis software system), version 12.0. www.statsoft.com.).

Computational Methods. Molecular docking of **3** into the D3R X-ray crystal structure, PDB ID: 3PBL,[50] was used to develop an understanding of its molecular mode of binding, SAR, and selectivity. The structure was prepared using the Protein Preparation Wizard in Maestro (version 9.7, Schrödinger, LLC, New York, NY, 2014) using default options following deletion of the T4-

lysozyme residues that replaced most of the third cytoplasmic loop (ICL3). Compound **3** was docked in its protonated form using Induced Fit Docking (Induced Fit Docking protocol 2014-1, Glide version 6.1, Prime version 3.4, Schrödinger, LLC, New York, NY, 2014)[49, 58] using the default options. The pose chosen for analysis was the lowest energy one that maintained a salt bridge between the basic amine of the morpholine of compounds **3** and the conserved Asp1103.32 of D3R, while also keeping compound **3** in hydrogen bonding proximity to Tyr361.39.

Associated Content

Acknowledgements. The authors thank Katherine Brighty for her insightful comments on this manuscript.

Supporting Information Available

This material is available free of charge via the Internet at http://pubs.acs.org.

Corresponding Author

*To whom correspondence should be addressed. Mailing address: Pfizer Worldwide Research and Development, 610 Main Street, Cambridge, MA 02139; Tel: 857-225-2840; Fax 860-686-6052; E-mail: travis.t.wager@pfizer.com

References

1. O'Connor, P. G., Sokol, R. J., and D'Onofrio, G. (2014) Addiction medicine: The birth of a new discipline, *JAMA Internal Medicine 174*, 1717-1718.
2. Degenhardt, L., Whiteford, H. A., Ferrari, A. J., Baxter, A. J., Charlson, F. J., Hall, W. D., Freedman, G., Burstein, R., Johns, N., Engell, R. E., Flaxman, A., Murray, C. J. L., and Vos, T. (2013) Global burden of disease attributable to illicit drug use and dependence: findings from the Global Burden of Disease Study 2010, *The Lancet 382*, 1564-1574.
3. Wager, T. T., Chandrasekaran, R. Y., Bradley, J., Rubitski, D., Berke, H., Mente, S., Butler, T., Doran, A., Chang, C., Fisher, K., Knafels, J., Liu, S., Ohren, J., Marconi, M.,

DeMarco, G., Sneed, B., Walton, K., Horton, D., Rosado, A., and Mead, A. (2014) Casein Kinase 1δ/ε Inhibitor PF-5006739 Attenuates Opioid Drug-Seeking Behavior, *ACS Chemical Neuroscience 5*, 1253-1265.

4. Sokoloff, P., Giros, B., Martres, M.-P., Bouthenet, M.-L., and Schwartz, J.-C. (1990) Molecular cloning and characterization of a novel dopamine receptor (D3) as a target for neuroleptics, *Nature 347*, 146-151.
5. Newman, A. H., Grundt, P., and Nader, M. A. (2005) Dopamine D3 receptor partial agonists and antagonists as potential drug abuse therapeutic agents, *Journal of medicinal chemistry 48*, 3663-3679.
6. Heidbreder, C. A., and Newman, A. H. (2010) Current perspectives on selective dopamine D3 receptor antagonists as pharmacotherapeutics for addictions and related disorders, *Annals of the New York Academy of Sciences 1187*, 4-34.
7. Cho, D., Zheng, M., and Kim, K.-M. (2010) Current perspectives on the selective regulation of dopamine D2 and D3 receptors, *Archives of Pharmacal Research 33*, 1521-1538.
8. Keck, T. M., John, W. S., Czoty, P. W., Nader, M. A., and Newman, A. H. (2015) Identifying Medication Targets for Psychostimulant Addiction: Unraveling the Dopamine D3 Receptor Hypothesis, *Journal of Medicinal Chemistry 58*, 5361-5380.
9. Gurevich, E. V., and Joyce, J. N. (1999) Distribution of Dopamine D3 Receptor Expressing Neurons in the Human Forebrain: Comparison with D2 Receptor Expressing Neurons, *Neuropsychopharmacology 20*, 60-80.
10. Robinson, Mike J. F., and Berridge, Kent C. (2013) Instant Transformation of Learned Repulsion into Motivational "Wanting", *Current Biology 23*, 282-289.
11. Koob, G. F., and Volkow, N. D. (2009) Neurocircuitry of Addiction, *Neuropsychopharmacology 35*, 217-238.
12. Ikemoto, S., and Wise, R. A. (2004) Mapping of chemical trigger zones for reward, *Neuropharmacology 47, Supplement 1*, 190-201.
13. Kravitz, A. V., Tomasi, D., LeBlanc, K. H., Baler, R., Volkow, N. D., Bonci, A., and Ferré, S. (2015) Cortico-striatal circuits: Novel therapeutic targets for substance use disorders, *Brain Research 1628, Part A*, 186-198.
14. Koob, G. F. (2006) The neurobiology of addiction: a neuroadaptational view relevant for diagnosis, *Addiction 101*, 23-30.
15. Staley, J. K., and Mash, D. C. (1996) Adaptive Increase in D3 Dopamine Receptors in the Brain Reward Circuits of Human Cocaine Fatalities, *The Journal of Neuroscience 16*, 6100-6106.
16. Mash, D. C., and Staley, J. K. (1999) D3 Dopamine and Kappa Opioid Receptor Alterations in Human Brain of Cocaine-overdose Victims, *Annals of the New York Academy of Sciences 877*, 507-522.
17. Segal, D. M., Moraes, C. T., and Mash, D. C. (1997) Up-regulation of D3 dopamine receptor mRNA in the nucleus accumbens of human cocaine fatalities, *Molecular Brain Research 45*, 335-339.
18. Boileau, I., Payer, D., Houle, S., Behzadi, A., Rusjan, P. M., Tong, J., Wilkins, D., Selby, P., George, T. P., Zack, M., Furukawa, Y., McCluskey, T., Wilson, A. A., and Kish, S. J. (2012) Higher Binding of the Dopamine D3 Receptor-Preferring Ligand [11C]-(+)-Propyl-Hexahydro-Naphtho-Oxazin in Methamphetamine Polydrug Users: A Positron Emission Tomography Study, *The Journal of Neuroscience 32*, 1353-1359.

19. Erritzoe, D., Tziortzi, A., Bargiela, D., Colasanti, A., Searle, G. E., Gunn, R. N., Beaver, J. D., Waldman, A., Nutt, D. J., Bani, M., Merlo-Pich, E., Rabiner, E. A., and Lingford-Hughes, A. (2014) In Vivo Imaging of Cerebral Dopamine D3 Receptors in Alcoholism, *Neuropsychopharmacology 39*, 1703-1712.
20. Pilla, M., Perachon, S., Sautel, F., Garrido, F., Mann, A., Wermuth, C. G., Schwartz, J.-C., Everitt, B. J., and Sokoloff, P. (1999) Selective inhibition of cocaine-seeking behaviour by a partial dopamine D3 receptor agonist, *Nature 400*, 371-375.
21. Román, V., Gyertyán, I., Sághy, K., Kiss, B., and Szombathelyi, Z. (2013) Cariprazine (RGH-188), a D3-preferring dopamine D3/D2 receptor partial agonist antipsychotic candidate demonstrates anti-abuse potential in rats, *Psychopharmacology 226*, 285-293.
22. Le Foll, B., Goldberg, S. R., and Sokoloff, P. (2005) The dopamine D3 receptor and drug dependence: Effects on reward or beyond?, *Neuropharmacology 49*, 525-541.
23. Caine, S. B., Koob, G. F., Parsons, L. H., Everitt, B. J., Schwartz, J.-C., and Sokoloff, P. (1997) D3 receptor test in vitro predicts decreased cocaine self-administration in rats, *NeuroReport 8*, 2373-2377.
24. Wicke, K., and Garcia-Ladona, J. (2001) The dopamine D3 receptor partial agonist, BP 897, is an antagonist at human dopamine D3 receptors and at rat somatodendritic dopamine D3 receptors, *European Journal of Pharmacology 424*, 85-90.
25. Vorel, S. R., Ashby, C. R., Paul, M., Liu, X., Hayes, R., Hagan, J. J., Middlemiss, D. N., Stemp, G., and Gardner, E. L. (2002) Dopamine D3 Receptor Antagonism Inhibits Cocaine-Seeking and Cocaine-Enhanced Brain Reward in Rats, *The Journal of Neuroscience 22*, 9595-9603.
26. Xi, Z.-X., and Gardner, E. L. (2007) Pharmacological Actions of NGB 2904, a Selective Dopamine D3 Receptor Antagonist, in Animal Models of Drug Addiction, *CNS Drug Reviews 13*, 240-259.
27. Hu, R., Song, R., Yang, R., Su, R., and Li, J. (2013) The dopamine D3 receptor antagonist YQA14 that inhibits the expression and drug-primed reactivation of morphine-induced conditioned place preference in rats, *European Journal of Pharmacology 720*, 212-217.
28. Boateng, C. A., Bakare, O. M., Zhan, J., Banala, A. K., Burzynski, C., Pommier, E., Keck, T. M., Donthamsetti, P., Javitch, J. A., Rais, R., Slusher, B. S., Xi, Z.-X., and Newman, A. H. (2015) High Affinity Dopamine D3 Receptor (D3R)-Selective Antagonists Attenuate Heroin Self-Administration in Wild-Type but not D3R Knockout Mice, *Journal of Medicinal Chemistry 58*, 6195-6213.
29. Galaj, E., Manuszak, M., Babic, S., Ananthan, S., and Ranaldi, R. (2015) The selective dopamine D3 receptor antagonist, SR 21502, reduces cue-induced reinstatement of heroin seeking and heroin conditioned place preference in rats, *Drug and Alcohol Dependence 156*, 228-233.
30. Kumar, V., Bonifazi, A., Ellenberger, M. P., Keck, T. M., Pommier, E., Rais, R., Slusher, B. S., Gardner, E., You, Z.-B., Xi, Z.-X., and Newman, A. H. (2016) Highly Selective Dopamine D3 Receptor (D3R) Antagonists and Partial Agonists Based on Eticlopride and the D3R Crystal Structure: New Leads for Opioid Dependence Treatment, *Journal of Medicinal Chemistry 59*, 7634-7650.
31. Mugnaini, M., Iavarone, L., Cavallini, P., Griffante, C., Oliosi, B., Savoia, C., Beaver, J., Rabiner, E. A., Micheli, F., Heidbreder, C., Andorn, A., Merlo Pich, E., and Bani, M.

(2013) Occupancy of Brain Dopamine D3 Receptors and Drug Craving: A Translational Approach, *Neuropsychopharmacology 38*, 302-312.

32. Rudmann, D. G., Mcnerney, M. E., Vandereide, S. L., Schemmer, J. K., Eversole, R. R., and Vonderfecht, S. L. (2004) Epididymal and Systemic Phospholipidosis in Rats and Dogs Treated with the Dopamine D3 Selective Antagonist PNU-177864, *Toxicologic Pathology 32*, 326-332.
33. Micheli, F., and Heidbreder, C. (2006) Selective Dopamine D3 Receptor Antagonist: A Review 2001-2005, *Recent Pat. CNS Drug Discovery 1*, 271-288.
34. Wager, T. T., Pettersen, B. A., Schmidt, A. W., Spracklin, D. K., Mente, S., Butler, T. W., Howard, H., Lettiere, D. J., Rubitski, D. M., Wong, D. F., Nedza, F. M., Nelson, F. R., Rollema, H., Raggon, J. W., Aubrecht, J., Freeman, J. K., Marcek, J. M., Cianfrogna, J., Cook, K. W., James, L. C., Chatman, L. A., Iredale, P. A., Banker, M. J., Homiski, M. L., Munzner, J. B., and Chandrasekaran, R. Y. (2011) Discovery of Two Clinical Histamine H3 Receptor Antagonists: trans-N-Ethyl-3-fluoro-3-[3-fluoro-4-(pyrrolidinylmethyl)phenyl]cyclobutanecarboxamide (PF-03654746) and trans-3-Fluoro-3-[3-fluoro-4-(pyrrolidin-1-ylmethyl)phenyl]-N-(2-methylpropyl)cyclobutanecarboxamide (PF-03654764), *Journal of Medicinal Chemistry 54*, 7602-7620.
35. Attkins, N., Betts, A., Hepworth, D., and Heatherington, A. C. (2010) Pharmacokinetics and elucidation of the rates and routes of N-glucuronidation of PF-592379, an oral dopamine 3 agonist in rat, dog, and human, *Xenobiotica 40*, 730-742.
36. Wager, T. T., Chandrasekaran, R. Y., Hou, X., Troutman, M. D., Verhoest, P. R., Villalobos, A., and Will, Y. (2010) Defining Desirable Central Nervous System Drug Space through the Alignment of Molecular Properties, in Vitro ADME, and Safety Attributes, *ACS Chem. Neurosci. 1*, 420-434.
37. Wager, T. T., Hou, X., Verhoest, P. R., and Villalobos, A. (2010) Moving beyond rules: The development of a central nervous system multiparameter optimization (CNS MPO) approach to enable alignment of druglike properties, *ACS Chem. Neurosci. 1*, 435-449.
38. Wager, T. T., Hou, X., Verhoest, P. R., and Villalobos, A. (2016) Central Nervous System Multiparameter Optimization Desirability: Application in Drug Discovery, *ACS Chemical Neuroscience 7*, 767-775.
39. Ben-Jonathan, N., Arbogast, L. A., and Hyde, J. F. (1989) Neuroendrocrine regulation of prolactin release, *Progress in neurobiology 33*, 399-447.
40. Rummel-Kluge, C., Komossa, K., Schwarz, S., Hunger, H., Schmid, F., Kissling, W., Davis, J. M., and Leucht, S. (2012) Second-Generation Antipsychotic Drugs and Extrapyramidal Side Effects: A Systematic Review and Meta-analysis of Head-to-Head Comparisons, *Schizophrenia Bulletin 38*, 167-177.
41. Coffin, V. L., Latranyi, M. B., and Chipkin, R. E. (1989) Acute extrapyramidal syndrome in Cebus monkeys: development mediated by dopamine D2 but not D1 receptors, *Journal of Pharmacology and Experimental Therapeutics 249*, 769-774.
42. Beart, P. (1988) Dopamine receptors (Vol. 8: Receptor biochemistry and methodology): edited by I. Creese and CM Fraser, Alan R. Liss, 1987.(ix+ 256 pages) ISBN 0 8451 3707 7, Elsevier Current Trends.
43. Hartesveldt, C. V., Cottrell, G. A., Potter, T., and Meyer, M. E. (1992) Effects of intracerebral quinpirole on locomotion in rats, *European Journal of Pharmacology 214*, 27-32.

44. Baron, J. C., Martinot, J. L., Cambon, H., Boulenger, J. P., Poirier, M. F., Caillard, V., Blin, J., Huret, J. D., Loc'h, C., and Maziere, B. (1989) Striatal dopamine receptor occupancy during and following withdrawal from neuroleptic treatment: correlative evaluation by positron emission tomography and plasma prolactin levels, *Psychopharmacology 99*, 463-472.
45. Kapur, S., Langlois, X., Vinken, P., Megens, A. A. H. P., De Coster, R., and Andrews, J. S. (2002) The Differential Effects of Atypical Antipsychotics on Prolactin Elevation Are Explained by Their Differential Blood-Brain Disposition: A Pharmacological Analysis in Rats, *Journal of Pharmacology and Experimental Therapeutics 302*, 1129-1134.
46. Gyertyán, I., and Sághy, K. (2007) The selective dopamine D3 receptor antagonists, SB 277011-A and S 33084 block haloperidol-induced catalepsy in rats, *European Journal of Pharmacology 572*, 171-174.
47. Maggio, R., Aloisi, G., Silvano, E., Rossi, M., and Millan, M. J. (2009) Heterodimerization of dopamine receptors: new insights into functional and therapeutic significance, *Parkinsonism & Related Disorders 15, Supplement 4*, S2-S7.
48. Maggio, R., Scarselli, M., Capannolo, M., and Millan, M. J. (2015) Novel dimensions of D3 receptor function: Focus on heterodimerisation, transactivation and allosteric modulation, *European Neuropsychopharmacology 25*, 1470-1479.
49. Sherman, W., Day, T., Jacobson, M. P., Friesner, R. A., and Farid, R. (2006) Novel Procedure for Modeling Ligand/Receptor Induced Fit Effects, *Journal of Medicinal Chemistry 49*, 534-553.
50. Chien, E. Y. T., Liu, W., Zhao, Q., Katritch, V., Won Han, G., Hanson, M. A., Shi, L., Newman, A. H., Javitch, J. A., Cherezov, V., and Stevens, R. C. (2010) Structure of the Human Dopamine D3 Receptor in Complex with a D2/D3 Selective Antagonist, *Science 330*, 1091-1095.
51. Marchant, N. J., Li, X., and Shaham, Y. (2013) Recent developments in animal models of drug relapse, *Current Opinion in Neurobiology 23*, 675-683.
52. Wager, T. T., Kormos, B. L., Brady, J. T., Will, Y., Aleo, M. D., Stedman, D. B., Kuhn, M., and Chandrasekaran, R. Y. (2013) Improving the Odds of Success in Drug Discovery: Choosing the Best Compounds for in Vivo Toxicology Studies, *Journal of Medicinal Chemistry 56*, 9771-9779.
53. Ertl, P. (2008) Polar surface area, *Methods Princ. Med. Chem. 37*, 111-126.
54. Feng, B., Mills Jessica, B., Davidson Ralph, E., Mireles Rouchelle, J., Janiszewski John, S., Troutman Matthew, D., and de Morais Sonia, M. (2008) In vitro P-glycoprotein assays to predict the in vivo interactions of P-glycoprotein with drugs in the central nervous system, *Drug Metab. Dispos. 36*, 268-275.
55. Hosea, N. A., Collard, W. T., Cole, S., Maurer, T. S., Fang, R. X., Jones, H., Kakar, S. M., Nakai, Y., Smith, B. J., Webster, R., and Beaumont, K. (2009) Prediction of human pharmacokinetics from preclinical information: comparative accuracy of quantitative prediction approaches, *J. Clin. Pharmacol. 49*, 513-533.
56. Gao, H., Yao, L., Mathieu, H. W., Zhang, Y., Maurer, T. S., Troutman, M. D., Scott, D. O., Ruggeri, R. B., and Lin, J. (2008) In silico modeling of nonspecific binding to human liver microsomes, *Drug Metab. Dispos. 36*, 2130-2135.
57. O'Connor, E. C., Parker, D., Rollema, H., and Mead, A. N. (2010) The α4β2 nicotinic acetylcholine-receptor partial agonist varenicline inhibits both nicotine self-

administration following repeated dosing and reinstatement of nicotine seeking in rats, *Psychopharmacology 208*, 365-376.

58. Sherman, W., Beard, H. S., and Farid, R. (2006) Use of an Induced Fit Receptor Structure in Virtual Screening, *Chemical Biology & Drug Design 67*, 83-84.

Graphical Abstract

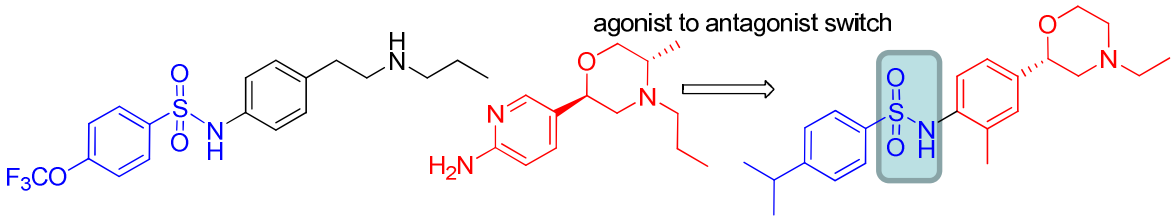

1 (PNU-177864)
D3 antagonist

2 (PF-592379)
D3 Agonist

3 (PF-4363467)
D3/D2 Antagonist

Dopamine D3/D2 Receptor Antagonist PF-04363467 Extinguishes and Blocks Opioid Drug-Seeking Behavior without Concomitant D2 Side Effects

Figures 1-6
Tables 1-4
Graphical Abstract

Table 1. Corporate file mining leads and tool compound **3**.

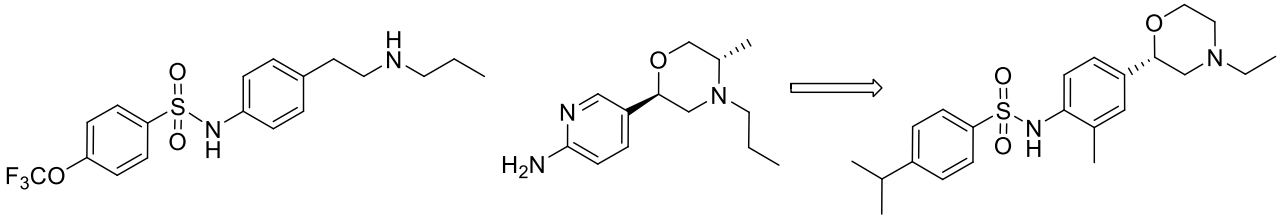

1 (PNU-177864) **2** (PF-592379) **3** (PF-4363467)

ID	D3 K_i (nM)[a]	D2 K_i (nM)[a]	D2/D3	D3 Functional (nM)[b]	D2 Functional (nM)[b]	Functional Activity
1	38.2 (23.6 – 61.9)	4480 (3290 – 6090)	117	K_i = 22 (10.1 - 48.9)[c]	K_i > 33[c]	Antagonist
2	322 (57.9 – 1790)	>4160	>12	EC_{50} = 21[d]	EC_{50} > 9,000[d]	Agonist
3	3.1 (2.47 – 3.99)	692 (539 – 890)	223	K_i = 1.1 (0.61 - 2.1)[c]	K_i = 464 (188 – 1147)[c]	Antagonist

[a]Human dopamine D3 and D2 binding data reported as the geometric mean of at least 3 determinations. [b]Human dopamine D3 and D2 functional data reported as the geometric mean of at least 3 determinations. [c]Data reported as mean antagonist activity with (95% CI). [d]Data reported by Attkins et al.[35] as agonist activity.

Table 2. Summary of physicochemical properties and CNS MPO desirability
[a]Calculated CNS MPO desirability scores were obtained using the published algorithm.[30]

	Compound **1**		Compound **2**		Compound **3**	
Physicochemical Property	Value	Component Score	Value	Component Score	Value	Component Score
MW	402	0.70	235	1.00	403	0.70
ClogP	4.46	0.27	1.48	1.00	4.06	0.47
TPSA	67.4	1.00	51.4	1.00	58.6	1.00
ClogD7.4	1.06	1.00	0.76	1.00	3.96	0.02
HBD	2	0.50	2	0.50	1	0.83
pK_a	10.6	0.00	7.5	1.00	7.5	1.00
CNS MPO		3.5/ 6.0		5.5/ 6.0		4.0/ 6.0

Table 3. Summary of ADME properties for **3**.

Compound	HLM[a]	P_{app}[b]	P-gp[c]	Rat $C_{max,b,u}$ [nM][d]	Rat $AUC_{0-\infty}$ C_b/C_p	Rat $AUC_{0-\infty}$ $C_{b,u}/C_{p,u}$
3	126	8.4	2.3	23.7	2.4	1.01

•[a]Human liver microsomal clearance (mL/min/mg). [b]Passive permeability (P_{app} AB x 10^{-6} cm/sec). [c]MDR1 Efflux Ratio (BA/AB). [d]Rat $C_{max,b,u}$ values are reported as maximum free drug concentration in brain at a 10 mg/kg dose, s.c.

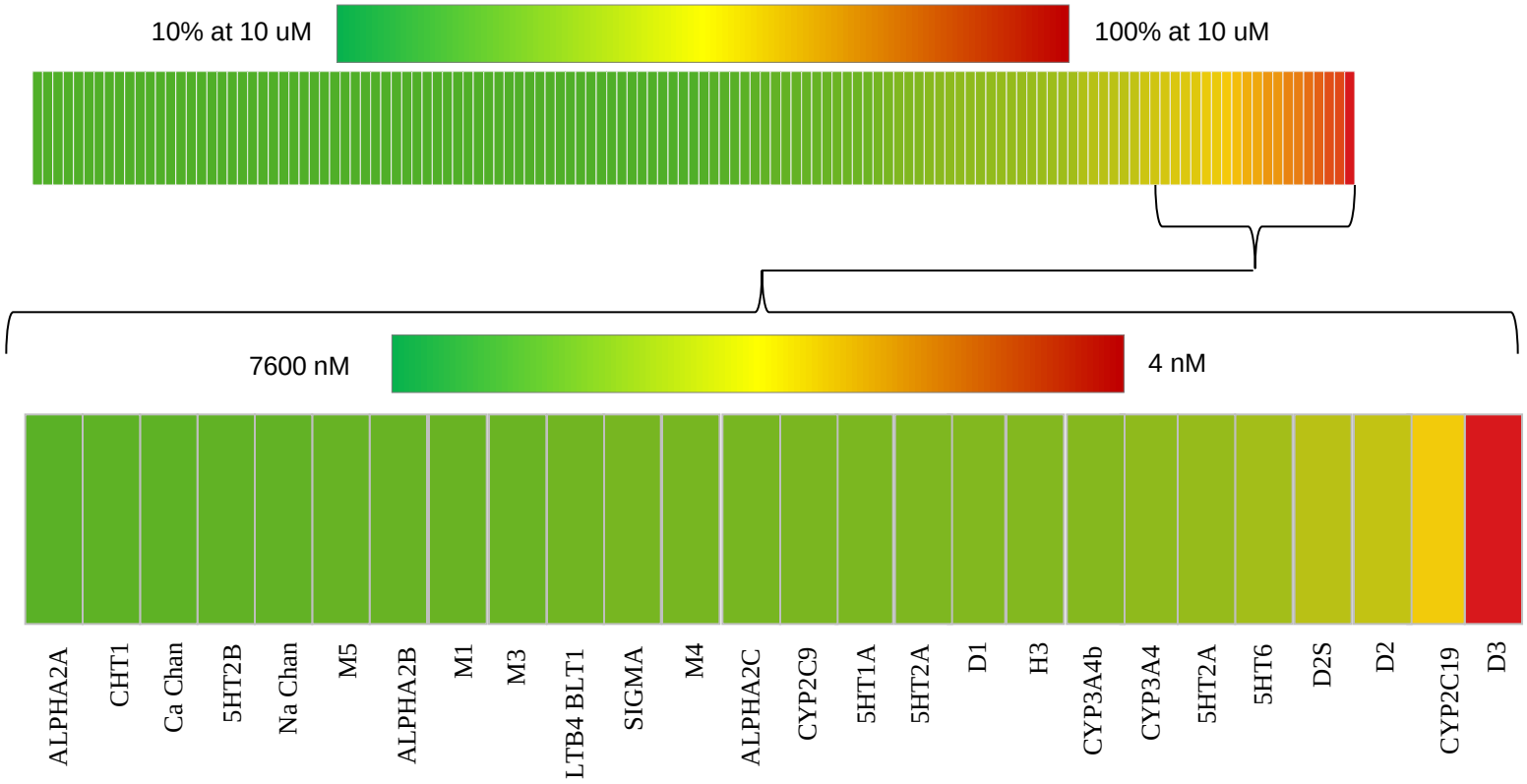

Figure 1. A) Percent inhibition of a 129-target promiscuity panel at 10 µM of compound **3**. Heat map colors for this continuum: green, 0% inhibition; yellow, 50% inhibition; red, 100% inhibition. B) IC_{50} determination for 26 targets hitting in the promiscuity panel with inhibition >50% for compound **3**. Heat map colors continuum: green, 7,600 nM; yellow, 100 nM and red, 4 nM. IC_{50} determinations for the 10 highest affinity targets for compound **3** were: D3R, 4 nM; CYP2C19, 110 nM; D2R, 420 nM; D2S, 540 nM; 5HT6, 990 nM; 5HT2A, 1400 nM; CYP3A4b, 2300 nM; H3, 2400 nM; D1R, 2500 nM.

Table 4. D3R and D2R brain receptor occupancy from autoradiography techniques in rats

Compound	Treatment	D3 EVRO % RO Observed[a]	D2 EVRO % RO Observed[b]
3	32 mg/kg	---	85.9 ± 1.7
	10 mg/kg	98.8 ± 2.4	50.6 ± 3.5
	3.2 mg/kg	99.9 ± 0.5	34.7 ± 1.5
	0.1 mg/kg	33.6 ± 4.5	10.8 ± 4.1
	0.03 mg/kg	6.3 ± 10.1	---
	EC_{50}	1.5 ± 0.4 nM	46.6 ± 9.1 nM

[a]Brain region evaluated: rat cerebellum (mean ± SEM, *n* = 3–4). [b]Brain region evaluated: rat striatum (mean ± SEM, *n* = 4). Ex vivo Receptor Occupancy (EVRO).

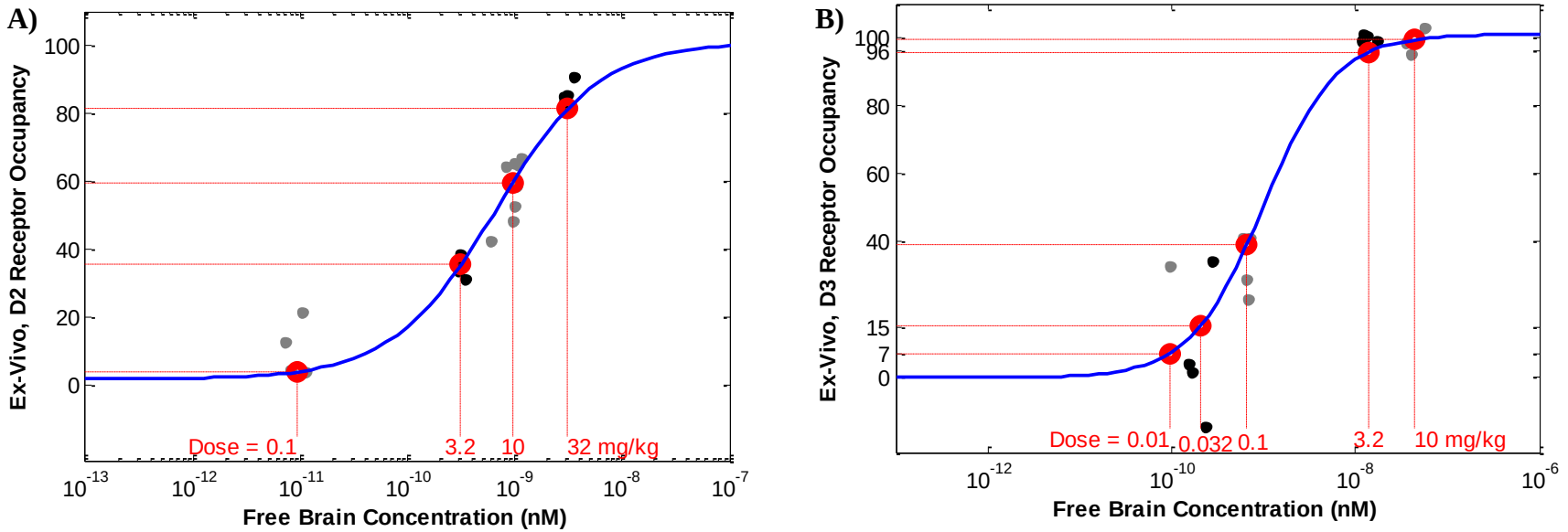

Figure 2. A) D2 (striatum) and B) D3 (cerebellum) brain receptor occupancy curves from the ex vivo autoradiography protocol in rat. The gray and black data points represent actual measured RO and brain PK from individual animals. The solid line is the data-fitted RO model. The D3R binding was measured in cerebellum, while the D2R binding was measured in striatum.

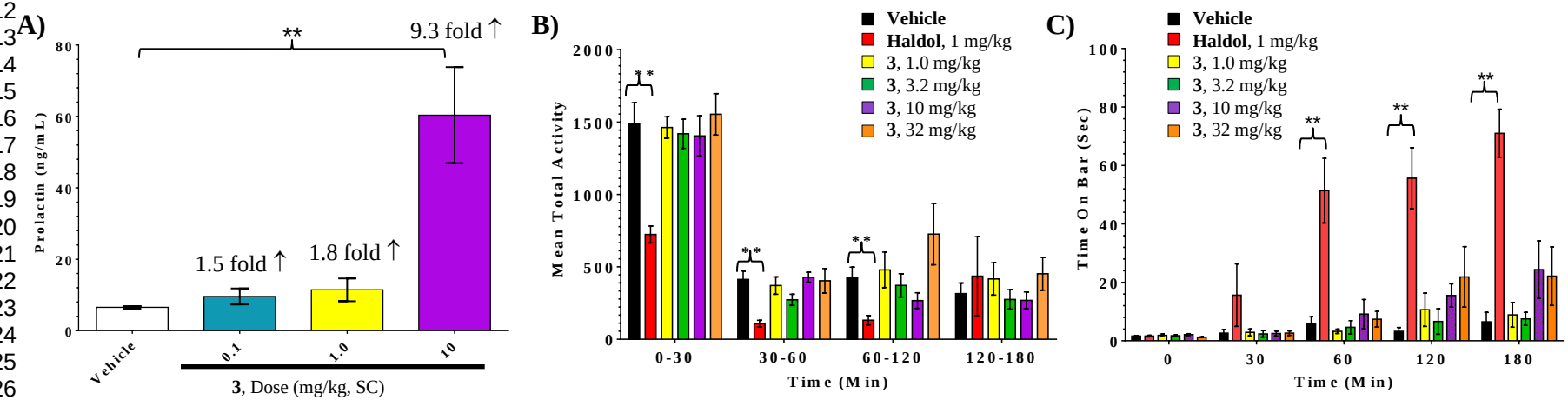

Figure 3. A) Effect of **3** on prolactin. Data represent mean ± SEM, *n* = 5/group. B) Effects of **3** on total activity in a rat model of locomotor activity. Data represent mean ± SEM locomotor activity over 30 minute time bins, *n* = 8/group. C) Effects of **3** in a rat model of catalepsy. Data represents mean ± SEM seconds on bar demonstrating the effect of **3** (1.0–32.0 mg/kg, s.c.), *n* = 8/group. ** indicates $p < 0.01$ compared to vehicle group.

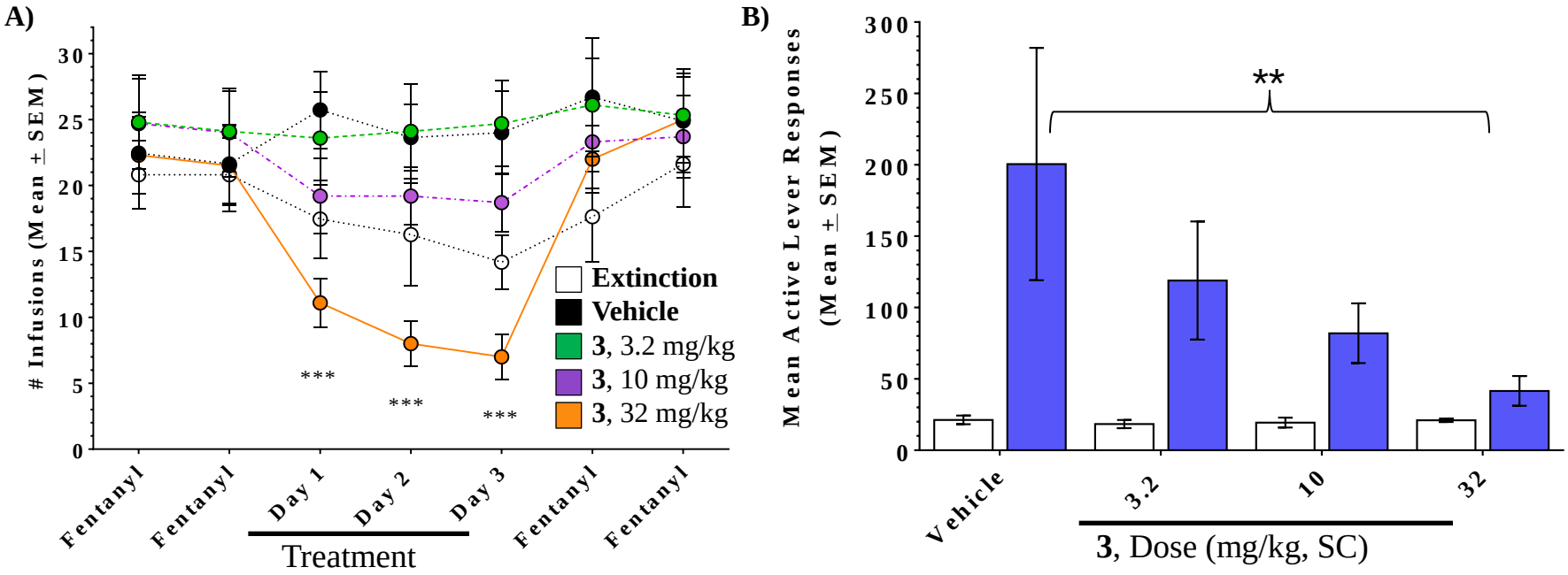

Figure 4. A) Effects of vehicle or **3** pretreatment on fentanyl self-administration over 3 test days in the rat model of cessation. Data represent the average infusions of fentanyl across baseline responding (fentanyl) before and after test sessions as well as three consecutive test sessions with **3** (Days 1–3). Saline extinction tests (Extinction) are also shown, in which saline was substituted for fentanyl during test sessions. n = 9–11; *** $p < 0.001$. B) Effects of **3** on combined cue and fentanyl prime-induced reinstatement of fentanyl-seeking behavior. Data represent mean ± SEM active lever responses, with white bars representing baseline active lever responses and blue bars representing active lever response on reinstatement test conditions. n = 8; ** $p < 0.01$

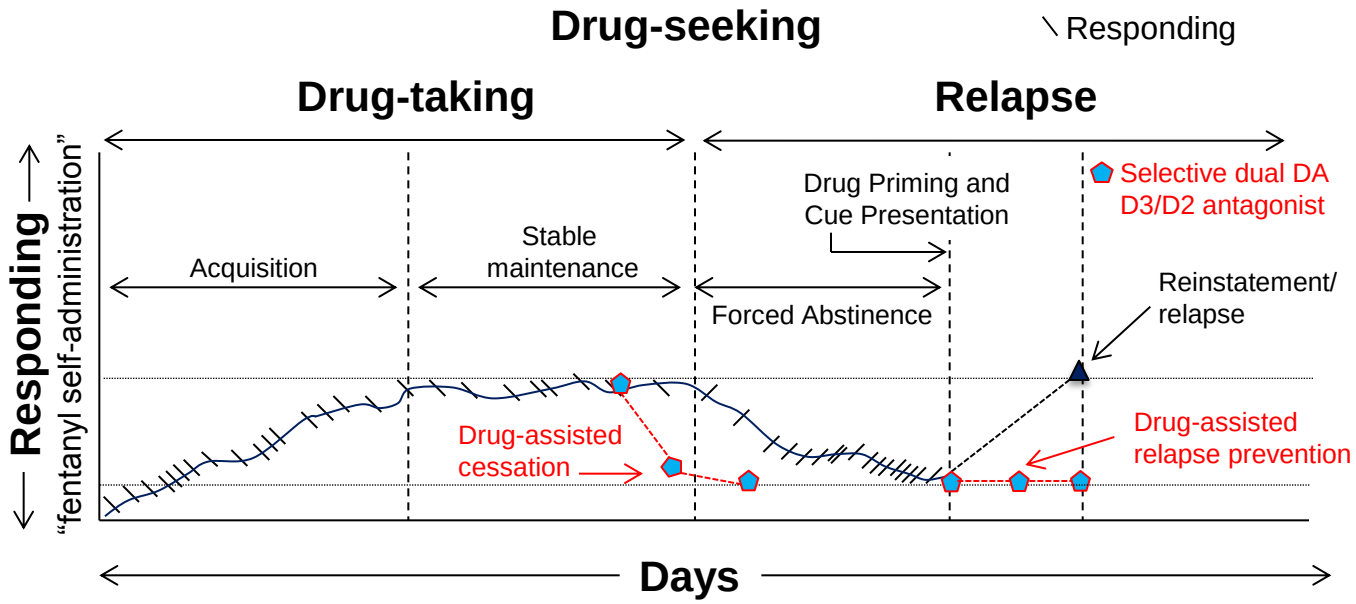

Figure 5. General depiction of the experiment. Selective D3/D2 antagonist **3** attenuates fentanyl-seeking behavior in models of both cessation of fentanyl self-administration and reinstatement (as a model of relapse).

Scheme 1: Synthesis of D3R/D2R antagonist **3**.

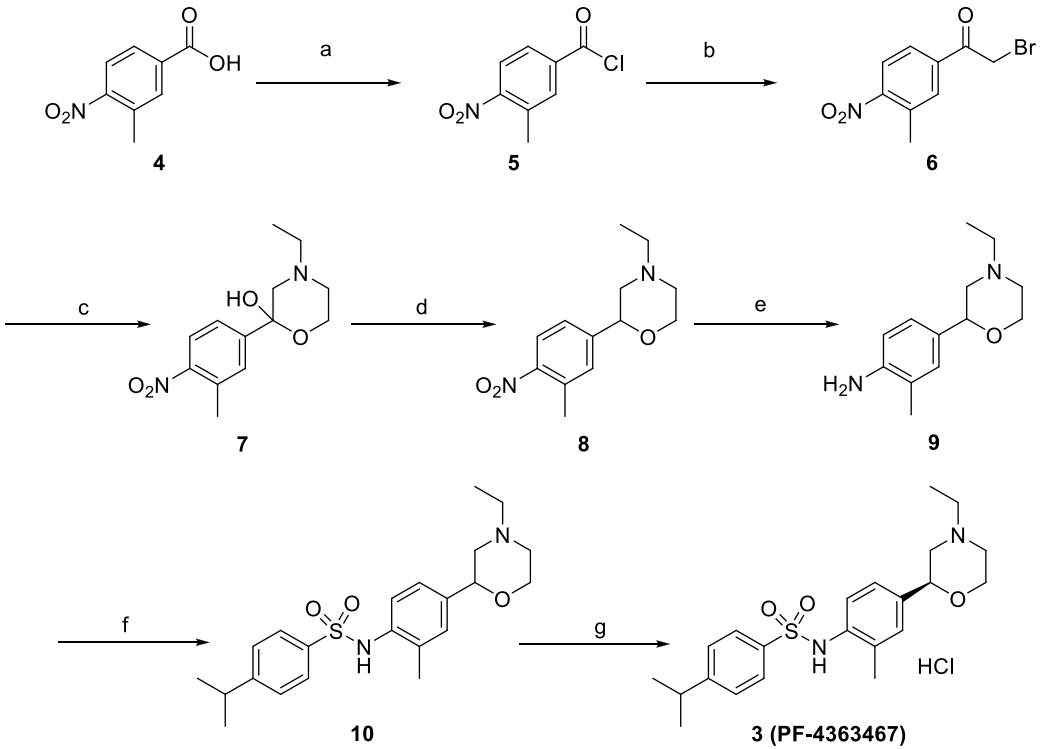

Reagents and conditions: a) thionyl chloride, DMF; b) (trimethylsilyl)diazomethane, ACN/THF, then 40% HBr; c) 2-(ethylamino)ethanol, Et_3N, CH_2Cl_2; d) triethylsilane, TFA, CH_2Cl_2; e) H_2, Raney Ni, MeOH; f) 4-isopropylbenzene-1-sulfonyl chloride, pyridine; g) chiral chromatographic separation, then HCl/EtOAc/Et_2O.

Graphical Abstract

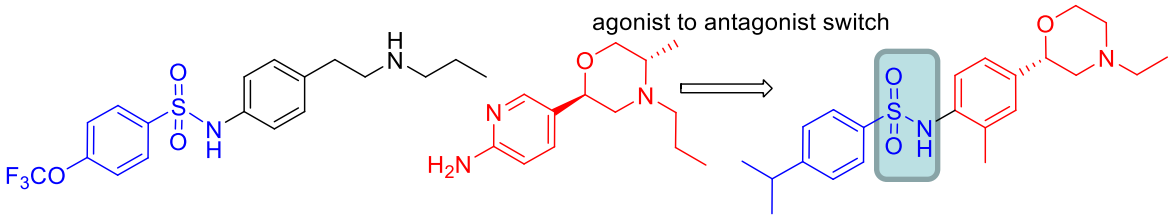

1 (PNU-177864)
D3 antagonist

2 (PF-592379)
D3 Agonist

3 (PF-4363467)
D3/D2 Antagonist